行政院國家科學委員會專題研究計畫 成果報告

以高分子作為感應偶合電漿反應離子蝕刻側壁保護層以製作單晶矽懸浮微結構之快速製程平台研發
研究成果報告(精簡版)

計 畫 類 別 ：個別型
計 畫 編 號 ：NSC 100-2221-E-009-034-
執 行 期 間 ：100 年 08 月 01 日至 101 年 07 月 31 日
執 行 單 位 ：國立交通大學機械工程學系（所）

計 畫 主 持 人：徐文祥

計畫參與人員：碩士班研究生-兼任助理人員：吳族豪
博士班研究生-兼任助理人員：吳松岳
博士班研究生-兼任助理人員：謝一全

報 告 附 件 ：出席國際會議研究心得報告及發表論文

公 開 資 訊 ：本計畫可公開查詢

中 華 民 國 101 年 10 月 03 日

中 文 摘 要 ： 本計畫根據單晶矽微加工技術之特點，提出以感應耦合電漿離子蝕刻（Inductively Coupled Plasma Reactive Ion Etching , ICP-RIE）之體型微加工製程技術，以高分子作為蝕刻保護層來製作單晶矽懸浮結構製程平台技術（Polymer Passivation Layer for Suspended structures Etching , PoPLSE），除黃光製程外，其餘製程均整合在 ICP-RIE 機台中完成，低溫製程、製程簡化、使用機台少及製程快速，為此製程平台之特點。

PoPLSE 製程平台研究分為非等向性蝕刻及等向性蝕刻兩部分，在非等向性蝕刻的部分，詳細探討 ICP-RIE 各項參數對蝕刻的影響，考量蝕刻之垂直度、側向蝕刻及蝕刻速率等規格，經基本參數優化後可得到深寬比達 30 且垂直度 89 ±1° 深寬比結構，並針對各種特殊需求，開發不同應用之最佳化製程參數。於等向性蝕刻的部分，探討高分子之保護效果，在不同結構開口尺寸下，高分子薄膜沈積、底部高分子薄膜去除及等向性蝕刻之各項參數關係，成功製作出結構厚度 30 μm 及 60 μm、結構線寬/開口為 5 μm 及 10 μm 之懸浮梳狀結構，驗證此製程平台之可行性。

中文關鍵詞： 感應耦合電漿、乾蝕刻、高分子、保護層、懸浮、單晶矽

英 文 摘 要 ： In recent year, MEMS products have been widely used in various industries, especially in the 3C manufactures. The rapid and stable fabrication platform technology of the process plays a very important role in industrial development. This paper presents a rapid bulk micromachining process named Polymer Passivation Layer for Suspended structures Etching (PoPLSE) by using polymer as protecting passivation layer at both anisotropic and isotropic etching steps. The proposed method can fabricate suspended single-crystal-silicon (SCS) structures in Inductively Coupled Plasma Reactive Ion Etching (ICP-RIE) chamber directly, which would simplify the fabrication process and save fabrication time.

In anisotropic silicon etching, the basic parameters have been systematical studied in the paper. For the different etching specifications, such as verticality, aspect-ratio, roughness, lateral etching and etching rate, etc., the optimum recipe of high-aspect-ratio etching process parameters have been

developed for different applications.
The current study systematically investigates critical fabrication parameters to verify feasibility of the proposed PoPLSE fabrication platform method, and discusses the polymer passivation time and removal time of polymer at the base of substrate at different opening gaps of 5, 10, 30, and 50 μm and different depths of 30 and 50 μm to establish suitable recipes for fabricating suspended structures. The suitable recipes for comb-drive microstructures with 30μm or 60μm in depth and 5μm or 10μm line width at different opening sizes are experimentally identified.

英文關鍵詞： ICP, dry etching, polymer, passivation, suspended, SCS

行政院國家科學委員會補助專題研究計畫 □期中進度報告 ■期末報告

以高分子作為感應偶合電漿反應離子蝕刻側壁保護以製作單晶矽懸浮微結構之快速製程平台研發

計畫類別：■個別型計畫　□整合型計畫
計畫編號：NSC　100－2221－E－009－034－
執行期間：　100 年 08 月 01 日至 101 年 07 月 31 日

執行機構及系所：國立交通大學機械系

計畫主持人：徐文祥
計畫協同研究人員:林郁欣
計畫參與人員：謝一全、王盈斌、吳族豪

本計畫除繳交成果報告外，另含下列出國報告，共 1 份：
□移地研究心得報告
■出席國際學術會議心得報告
□國際合作研究計畫國外研究報告

處理方式：除列管計畫及下列情形者外，得立即公開查詢
□涉及專利或其他智慧財產權，□一年□二年後可公開查詢

中　華　民　國 101 年 07 月 31 日

1. 摘要

本計畫根據單晶矽微加工技術之特點，提出以感應耦合電漿離子蝕刻（Inductively Coupled Plasma Reactive Ion Etching , ICP-RIE）之體型微加工製程技術，以高分子作為蝕刻保護層來製作單晶矽懸浮結構製程平台技術（Polymer Passivation Layer for Suspended structures Etching , PoPLSE），除黃光製程外，其餘製程均整合在 ICP-RIE 機台中完成，低溫製程、製程簡化、使用機台少及製程快速，為此製程平台之特點。

PoPLSE 製程平台研究分為非等向性蝕刻及等向性蝕刻兩部分，在非等向性蝕刻的部分，詳細探討 ICP-RIE 各項參數對蝕刻的影響，考量蝕刻之垂直度、側向蝕刻及蝕刻速率等規格，經基本參數優化後可得到深寬比達 30 且垂直度 89 ±1°之高深寬比結構，並針對各種特殊需求，開發不同應用之最佳化製程參數。於等向性蝕刻的部分，探討高分子之保護效果，在不同結構開口尺寸下，高分子薄膜沈積、底部高分子薄膜去除及等向性蝕刻之各項參數關係，成功製作出結構厚度 30 μm 及 60 μm、結構線寬/開口為 5 μm 及 10 μm 之懸浮梳狀結構，驗證此製程平台之可行性。

In recent year, MEMS products have been widely used in various industries, especially in the 3C manufactures. The rapid and stable fabrication platform technology of the process plays a very important role in industrial development. This paper presents a rapid bulk micromachining process named Polymer Passivation Layer for Suspended structures Etching (PoPLSE) by using polymer as protecting passivation layer at both anisotropic and isotropic etching steps. The proposed method can fabricate suspended single-crystal-silicon (SCS) structures in Inductively Coupled Plasma Reactive Ion Etching (ICP-RIE) chamber directly, which would simplify the fabrication process and save fabrication time.

In anisotropic silicon etching, the basic parameters have been systematical studied in the paper. For the different etching specifications, such as verticality, aspect-ratio, roughness, lateral etching and etching rate, etc., the optimum recipe of high-aspect-ratio etching process parameters have been developed for different applications.

The current study systematically investigates critical fabrication parameters to verify feasibility of the proposed PoPLSE fabrication platform method, and discusses the polymer passivation time and removal time of polymer at the base of substrate at different opening gaps of 5, 10, 30, and 50 μm and different depths of 30 and 50 μm to establish suitable recipes for fabricating suspended structures. The suitable recipes for comb-drive microstructures with 30μm or 60μm in depth and 5μm or 10μm line width at different opening

sizes are experimentally identified.

2. 計畫緣起與目的

微機電系統（Microelectromechanical system， MEMS）為結合機械、電子、材料、化學、生醫及光電等領域整合之微型化系統科技。起源於半導體製程技術，進而發展成為獨立之微機電製程技術，有別於半導體 2D 薄膜製程之面型微加工技術，微機電 3D 立體結構製程之體型微加工技術，更具特色及應用性。微機電立體結構的優點，包含體積、質量的增加及驅動力的提升等等，因此，高深寬比微加工技術（High Aspect Ratio Micromachining，HARM）應運而生，尤其是加工在單晶矽這個材料上的製程技術，備受重視，其原因為單晶矽對微機電系統而言為極佳之機械材料，除材料穩定外、結構剛性佳、加工無應力殘留、成本低、容易取得及與半導體製程相容等特點，使得此材料大量應用在各項產品上。

近年來微機電產品已大量上市於一般消費者市場中，例如汽車工業胎壓計之微壓力感測器、安全氣囊啟動之微加速度計、印表機之微噴墨頭、投影機之微光學元件、光通訊所使用之光開關、微光衰減器、微光柵及 RF 射頻感測元件等，還有最夯、最熱之各項消費性 3C 電子產品，如智慧型手機、平台電腦及 IPAD 中的微麥克風、微喇吧及微陀螺儀等等，這些微感測器及微致動器所應用之各種不同功能的產品，探究其核心材料及機械結構，有極大部分產品，皆使用單晶矽且為”懸浮可動”之機械結構所構成，利用這些懸浮的機械結構，作為感測各類訊號的改變，如電阻、電感、加速度及頻率等，或利用不同驅動方式，如靜電、熱力、磁力及壓電等來產生結構位移及形狀改變。隨著加工技術能力的提升，更小的線寬尺寸及更深的結構厚度，也就是所謂的深寬比不斷的被提高，結構深寬比提高可以提升元件的效能，以加速度計為例，可以增加感測之質量塊，提高感測器的靈敏度，以靜電梳狀致動器為例，可提高致動器的輸出力或降低驅動電壓等。但是，懸浮結構深寬比的提高，使得微加工製作技術在製作懸浮結構上的困難度增加。雖然高深寬比懸浮結構之產品應用性極廣，但製程流程複雜、製程冗長且製作難度高，因此，簡單、快速、穩定製作懸浮可動結構之製程平台技術極為重要。

單晶矽（Single-crystal-silicon, SCS）為半導體製程所製作電子電路元件之基本材料，且擁有極佳之機械及材料特性[1,2]，在所有材料當中，是最為符合微機電系統結合電子電路及機械結構特徵之材料，也因此應用極度廣泛。一般而言，矽基微加工分為濕式蝕刻與乾式蝕刻兩種，濕式蝕刻又可分為化學蝕刻及電化學蝕刻，氫氧化鉀(KOH)及氫氧化四甲基銨(TMAH)為傳統化學蝕刻中最基本之兩種蝕刻溶液，因為不同的晶片晶格方向會有不同的蝕刻速率，因此，單晶矽會蝕刻出特定結構形狀[3]，不同的蝕刻配方及參數也會影響蝕刻出的形貌[4-12]。另一種化學蝕刻方法為觸媒化學蝕刻，加入反應觸

媒，使單晶矽呈現非等向性蝕刻或多孔隙單晶矽蝕刻[13-16]。電化學蝕刻則是利用電場來輔助化學蝕刻，常使用於多孔隙單晶矽的製作[17]。濕式蝕刻因受晶片的晶格方向及蝕刻特性的影響，只能製作出一些簡單結構，因此，加工應用性受限。而乾式蝕刻為電漿離子蝕刻，加工圖形由光罩黃光微影定義，無結構圖形限制，傳統的離子蝕刻（Reactive Ion Etching, RIE）[18]，蝕刻速率慢<1 μm/min 且蝕刻垂直度較差，隨著高電漿離子濃度及低製程壓力製程技術的開發[19]，加上 Bosch 交替蝕刻之製程專利[20]，感應耦合電漿離子蝕刻（Inductively Coupled Plasma Reactive Ion Etching, ICP-RIE）被發展出來[21, 22]，不僅蝕刻速率提升至 3~5 μm/min，垂直度 90±1°，在高速蝕刻機台及參數下，蝕刻速率可高達 20 μm/min，因無加工圖形限制、蝕刻速率快及垂直度佳，使得目前 ICP-RIE 製程技術，在製作各種高深寬比之單晶矽微結構上，扮演舉足輕重的角色。雖 ICP-RIE 機台設備不便宜，但隨著蝕刻技術的發展及機台的普及，蝕刻製程成本也降低到能被接受的範圍，同時，各種單晶矽微機電產品的問市，也反映出 ICP-RIE 此技術值得發展的潛力。

由於單晶矽懸浮結構在微感測器及微致動器的應用廣泛，文獻上，許多製作懸浮結構製程平台技術，在很早期就被開發出來，以製程特性來分類，大致上可分為三種不同製程類型，如圖 2-1 所示，分為犧牲層型 SOI[23-25] 、結構填入型 Deep etching/Shallow diffusion[26]、HEXSIL[27] 及 HARPSS[28] ，如圖 2-2 所示，結構保護型 SCREAM[29, 30]、SBM[31]及 BELST[32, 33]，如圖 2-3 所示。

犧牲層型是選用訂製的特殊晶片（Silicon on Insulator, SOI），SOI 晶片為矽-二氧化矽-矽三層結構所構成，上方為單晶矽結構層，中間為二氧化作為矽絕緣層或犧牲層，底層為單晶矽基板，利用非等向性離子蝕刻結構層後，再將中間之二氧化矽當作犧牲層蝕刻掉，即可製作出懸浮結構，製程簡便及快速，但 SOI 晶片費用昂貴，成本考量導致此製程方式無法普及。

結構填入型是利用非等向性離子蝕刻出結構模型後，其中一種製程是利用摻雜硼的方式，摻雜硼的單晶矽與純單晶矽有蝕刻選擇比的差異，因此，蝕刻純單晶矽而留下不被蝕刻有摻雜硼的單晶矽部分，以摻雜硼的單晶矽作為懸浮結構，如圖 2-2(a)。另外方法是利用先填入二氧化矽當作犧牲層，再填入 Poly-silicon 當主要結構，將二氧化矽蝕刻掉而拿出 Poli-Siliocn 主要結構（圖 2-2(b)）或直接形成懸浮結構（圖 2-2(c)）。結構填入型的製程步驟繁瑣且複雜。

結構保護型是利用一層保護材料包覆住單晶矽結構，避免懸浮蝕刻製程時，蝕刻到單晶矽結構，一般以蝕刻選擇比較高之二氧化矽（SiO_2）或硼摻雜層（Boron Doping）來當作保護材料，大致來說，製程流程較結構填入型簡便，但因 SiO_2 或 Boron Doping 都是為高溫爐管製程所製作，因為高溫，使得

其他搭配的製程材料及製程方式變為複雜。

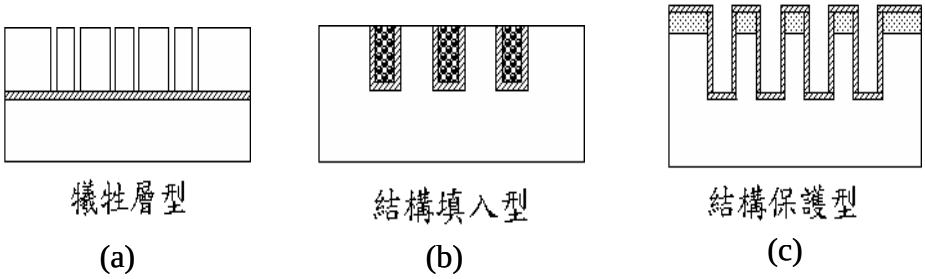

圖 2-1 懸浮結構製程平台技術 (a)犧牲層型 (b)結構填入型 (c)結構保護型

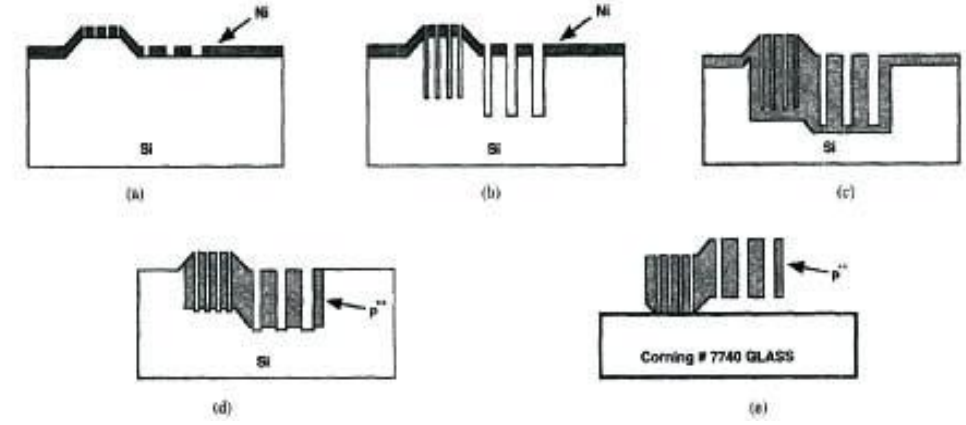

(a)

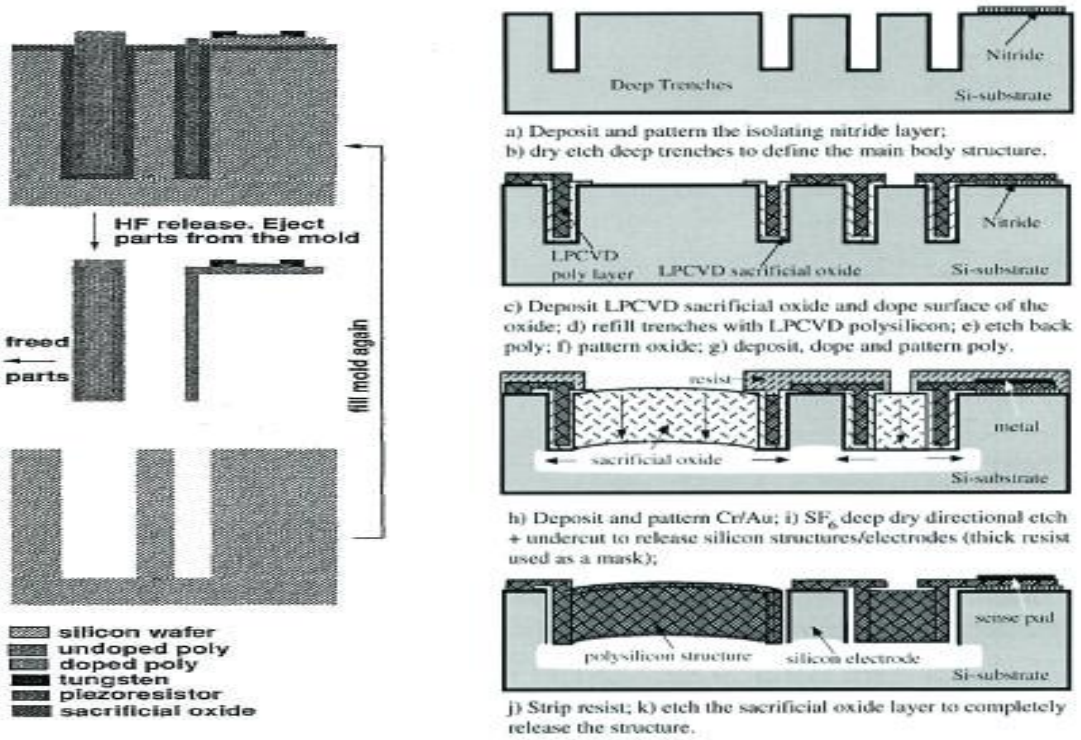

(b) (c)

圖 2-2 結構填入型製程技術 (a) Deep etching/shallow diffusion (b) HEXSIL (c) HARPSS

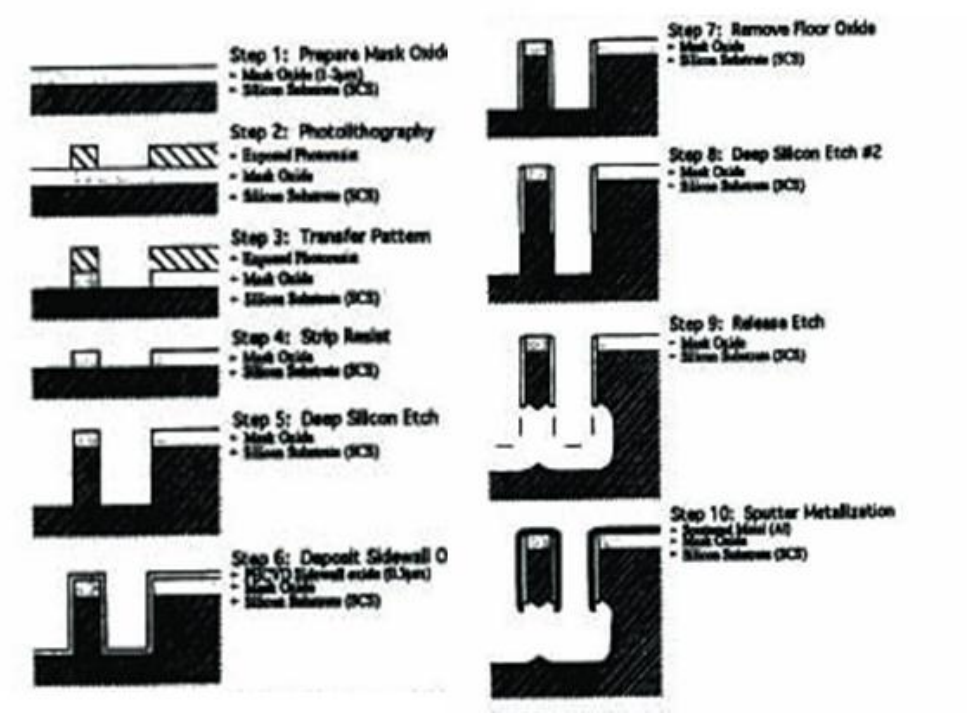

(a)

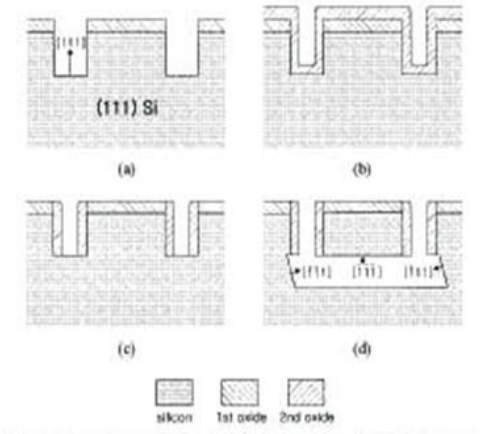

(b)

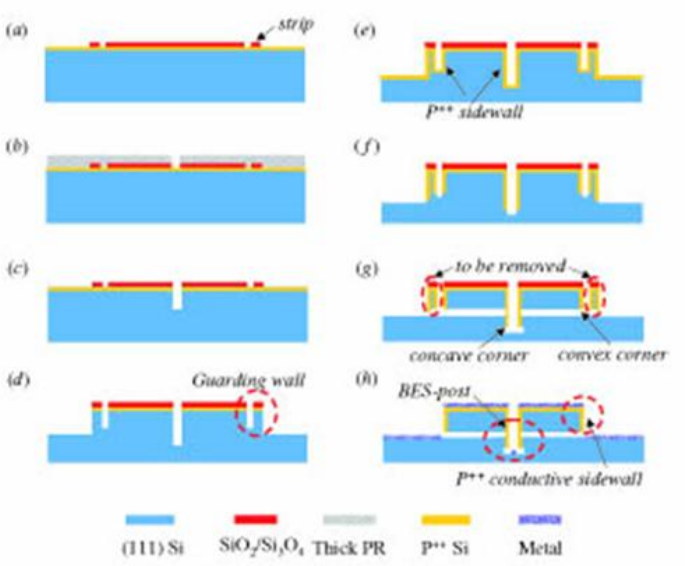

(c)

圖 2-3 結構保護型製程技術(a) SCREAM (b)Surface/Bulk Micromachine (SBM) (c)BELST

彙整上述文獻中所討論製作懸浮結構製程技術的方法，如表 2-1 所示，在非等向性蝕刻上，全是利用電漿離子蝕刻來達成，可見電漿離子蝕刻的重要性。犧牲層型 SOI 晶片成本太高，結構填入型因製程太過複雜，而結構保護型使用一般晶片且製程相較簡化，各自有特色。目前，若無成本考量，一般研究人員仍選擇用 SOI 晶片來製作懸浮結構，其主要原因為製程時程短，可快速驗證設計。因此，若能有一快速體型微加工製程平台，使用一般晶片製程降低成本，簡化製程機台來縮短製程時程，則能加速創新的設計實現。

表 2-1 懸浮製程技術比較

	結構保護型			結構填入型			犧牲層型
Process	SCREAM <100>	SBM <111>	BELST <111>	Etch/ Diffusion	HEXSIL	HARPSS	SOI
保護材料	SiO_2	SiO_2	Boron				
製程溫度	高溫	高溫	高溫	高溫	高溫	高溫	低溫
機台種類/使用機台次數	5/8	5/8	7/14	8/13	5/8	8/20	3/3
製程時程	冗長	冗長	冗長	冗長	冗長	冗長	快速
晶片成本（元/單片）	300~500	1000~2000	1000~2000	300~500	300~500	300~500	10,000
懸浮步驟	乾蝕刻	濕蝕刻	濕蝕刻	濕蝕刻	濕蝕刻	濕蝕刻	濕蝕刻

3. PoPLSE 製程平台

3.1. PoPLSE 製程設計與方法

以高分子作為蝕刻保護層來製作單晶矽懸浮結構 （Polymer Passivation Layer for Suspended structures Etching，PoPLSE）製程平台技術，是屬於結構保護型的製作方法之一。ICP-RIE 機台中之高分子材料原是作為非等向性蝕刻用途，並無使用在對等向性蝕刻的保護層。PoPLSE 製程同時以高分子材料作為非等向性及等向性蝕刻之保護層，除黃光製程外，其餘製程皆整合在 ICP-RIE 機台中完成。製作懸浮結構最關鍵之製程部分，即是保護層的步驟，標準 ICP-RIE Bosch 製程交替蝕刻中，高分子(CF_2)原是用來當作提高非等向性蝕刻目的之鈍化膜，在非等向性蝕刻後，側壁上雖有一層高分子材料，但此層高分子保護膜是無法直接抵擋長時間的等向性蝕刻，因此，需要額外的保護膜製程，才能製作出懸浮結構，因此，相關基本製程參數的研究極為重要。

本論文提出以高分子作為製作懸浮結構之保護層，其中的製程步驟，大致可分為非等向性蝕刻及等向性蝕刻。因為高分子沈積與去除為電漿離子態的製程方式，加上非等向性蝕刻及等向性蝕刻步驟，

全部製程步驟皆為電漿離子態形式，可說是全電漿製程流程，同時電漿離子製程過程中，雖然離子蝕刻會有熱反應的產生，但晶片背面有氦氣作為冷卻氣體，可讓製程溫度維持在 45 度之低溫製程。

PoPLSE 製程流程圖，如圖 3-1 所示，此製程選用一般單拋矽晶片< 100 >來製作，首先，進行標準 RCA clean 矽晶片後，旋塗正型光阻(AZ4620) 在矽晶片，黃光微影完成結構圖形當作後續蝕刻的遮罩及結構上方保護層，如圖 3-1(a)，之後的製程步驟則全部在 ICP-RIE 機台製程腔體中進行，如圖 3-1(b)至圖 3-1(f)。圖 3-1(b)為進行非等向性蝕刻，此蝕刻深度決定懸浮結構之厚度，然後進行等向性高分子薄膜沈積，將矽結構包覆起來（如圖 3-1(c)），再用非等向性蝕刻將底部高分子薄膜移除，此時可選擇是否加入氧氣或氫氣於蝕刻氣體中，幫助移除底部高分子薄膜，同時往矽基材下方蝕刻一些深度，此步驟幫助移除結構底部的矽材能順利進行（如圖 3-1(d)）；最後，進行等向性蝕刻，利用底切效應移除矽材結構底部材料，形成懸浮結構（如圖 3-1(e)），即完成懸浮結構製作。若要將光阻及高分子薄膜移除的話，可以通入氧電漿來去除（圖 3-1(f)）。另外，若後續需濺鍍金屬層當驅動電極，未避免矽材導通，可以重新再沈積一層高分子薄膜當作金屬電極層與矽材間的絕緣層。為避免不同開口尺寸，因蝕刻延遲及質傳效應導致結構蝕刻深度不同的問題，可於主要結構旁加入獨立的擋塊，使蝕刻的開口一致，獨立的擋塊結構在等向性蝕刻後，因與基板無連著，可輕易移除。

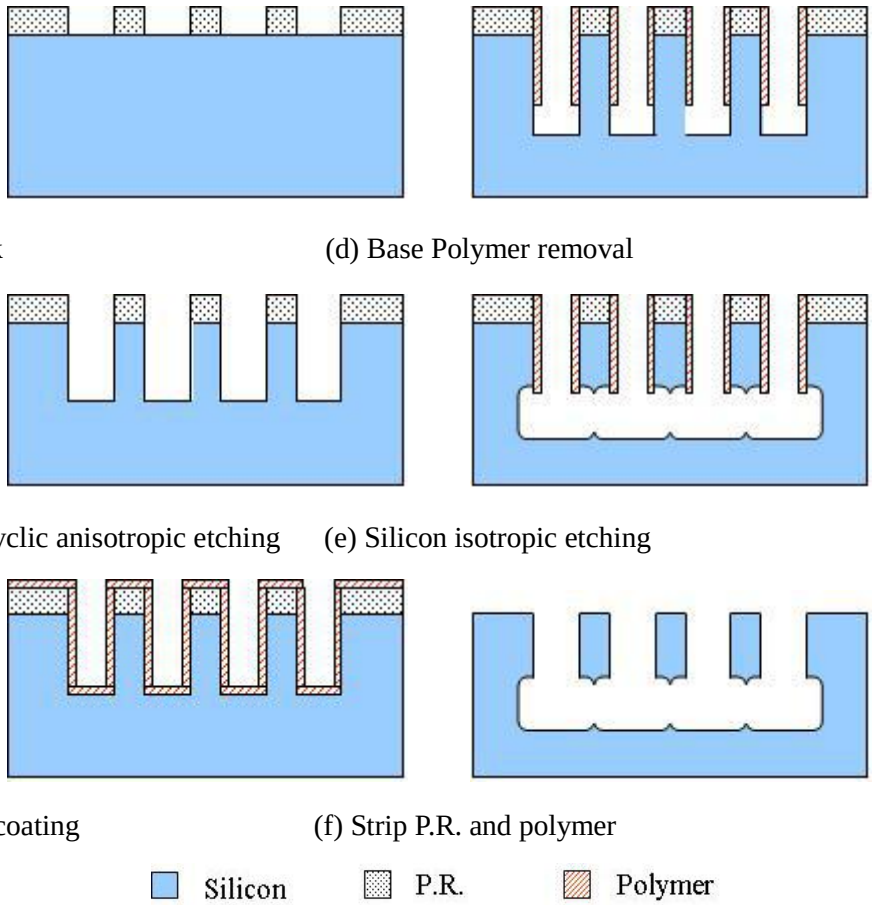

圖 3-1 PoPLSE 製程平台流程圖

3.2. ICP-RIE 各基本製程參數之影響

ICP-RIE 的參數非常多，影響蝕刻結果的參數有反應氣體的種類、氣體流量及時間、上/下電極的功率、製程腔體的壓力及軟體上的控制，如 overrun time 及 Ramp 功能。上電極：為提供氣體解離的能量，獲得所需的電漿離子，上電極功率越高氣體解離效率越好，獲得有效的電漿離子濃度越高。下電極：為提供腔體內一靜電偏壓，使帶電的電漿離子受偏壓吸引，而具有方向性的移動，同時增加物理性轟擊的效果，下電極功率增加則離子轟擊越強，若不施加下電極，則電漿離子在腔體內以擴散方式呈等向性的移動。氣體：為蝕刻與保護機制電漿離子的來源，在矽蝕刻中目前以 SF_6/C_4F_8 為主要蝕刻與保護氣體為主。而蝕刻與保護時間：控制每一個蝕刻週期時間，可改變側壁波紋的大小，時間越短的蝕刻保護週期，可以獲得較佳的側壁粗糙度。Overrun 時間：蝕刻與保護有重疊通入的時間，可緩和側壁波紋的大小，降低側壁粗糙度。Ramp：以每一週期為單位，隨之增加或減少時間的軟體功能，一般而言，蝕刻深度越深時，因質傳效果影響，使得結構越深，每一週期蝕刻的深度越淺，Ramp 功能可依每週期增加一定比例通入的時間，來補償因蝕刻深度變深，導致每一週期蝕刻之深度不同。除了蝕刻參數的因素外，影響蝕刻品質的因素，還有矽晶片規格、遮罩材料的種類、蝕刻的面積大小及不同開口的結構，均會導致蝕刻結果的不同，所以也需一併考量。

ICP-RIE 是利用 Bosch 交替蝕刻機制來進行非等向性矽深蝕刻，因此，在蝕刻側壁會產生如波紋之結構形貌，如圖 3-2(a)所示，側壁波紋為蝕刻保護交替蝕刻下所產生的正常現象，因側壁粗糙度欠佳，在一些光學元件、單晶矽模仁及高靈敏度感測器上，則無法使用。圖 3-2(b)為不同的開口尺寸下，蝕刻深度不同之情形，在同一片蝕刻晶片中，不同開口尺寸的結構，因質傳等因素導致蝕刻速率明顯不同，此稱為活性離子蝕刻延遲現象（Etching Lag）[34,35]，可加入補償結構，讓蝕刻開口尺寸一致，避免蝕刻延遲的現象。圖 3-3(a)則為底部側蝕的 Notch 現象，常發生於 SOI 晶片或穿孔蝕刻製程中，Notch 發生的原因是蝕刻底部為介電材料，導致電荷累積在介電材料的表面上，與電漿離子因同電荷相斥，反彈至側向矽材料上，時間越久側蝕情形越嚴重[36,37]。圖 3-3(b)則為結構偏上方被蝕刻成碗狀形狀，其原因為結構偏上方處，承受較多因光阻結構影響行進方向而來之離子攻擊，當蝕刻效果大於保護效果時，即會產生側壁碗狀形狀[38]。

良好的非等向性蝕刻，需由適當的蝕刻與保護比例才能達成，蝕刻與保護的比例不對，將直接影響蝕刻的結構垂直度，如圖 3-4 所示，蝕刻效果大於保護的比例，蝕刻結構將形成結構底部外擴的情形，如圖 3-4 (a)，相反地，蝕刻效果小於保護的比例，則結構將形成底部結構內凹的情況，如圖 3-4 (b)。反應電漿離子濃度不足時，輕微導致蝕刻之粗糙度變差，嚴重時側壁粗糙變糟及結構底部出現雜草的

現象，如圖 3-4(c)。遮罩的選擇也會影響蝕刻，當選用較軟性的材料如光阻時，因光阻邊角較容易被離子轟擊移除，因此容易產生結構上部側蝕的情況，硬質的遮罩材料如 SiO_2 及 Si_3N_4 則能降低此現象。

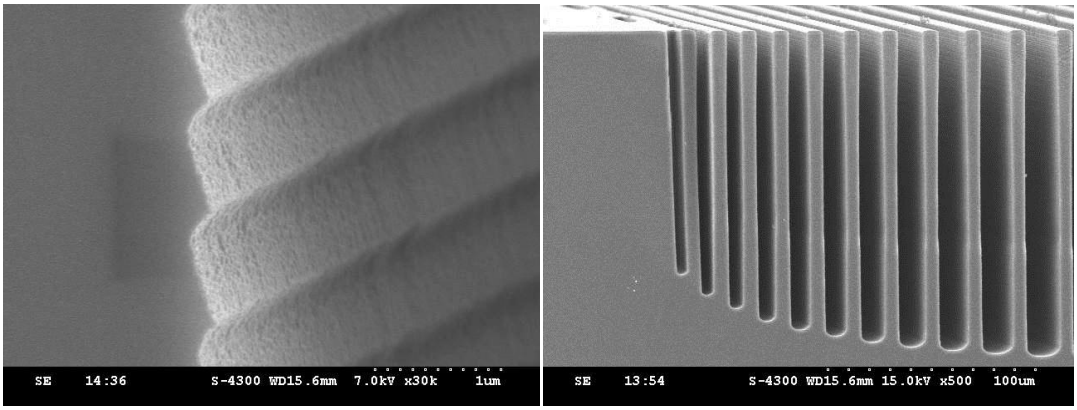

(a) (b)

圖 3-2 (a)側壁波紋結構 (b)因蝕刻延遲效應導致蝕刻深度不一

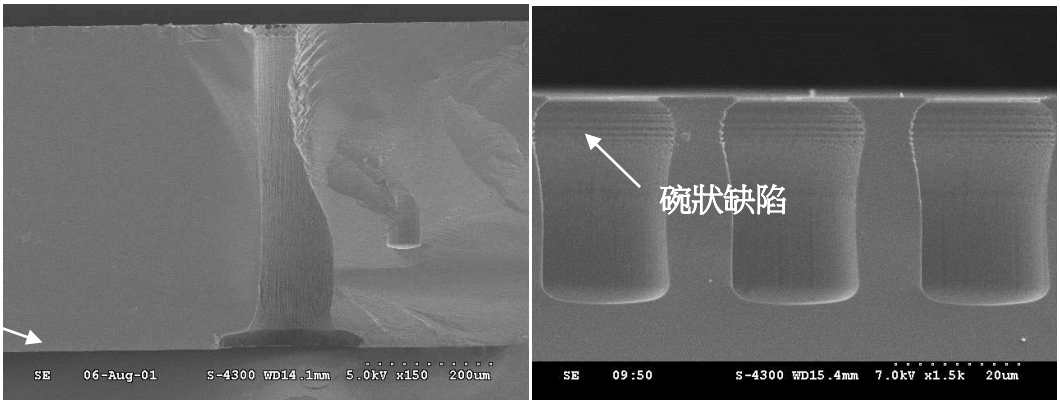

(a) (b)

圖 3-3 (a) Notch 效應導致蝕刻底部側蝕情形 (b)受光阻結構影響離子行進方向導致之側壁碗狀缺陷

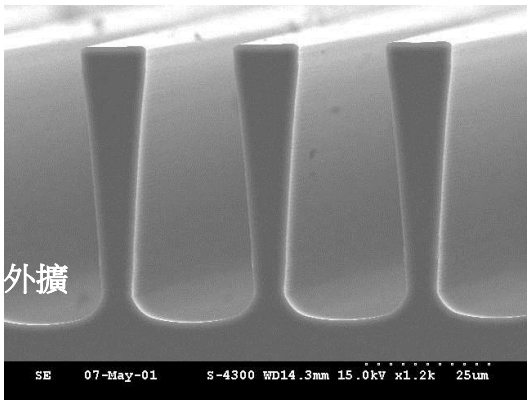

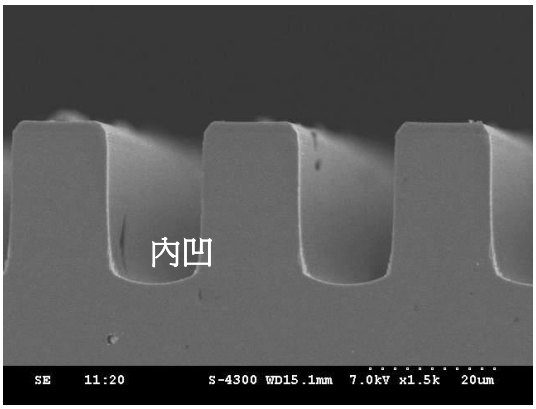

(a) (b)

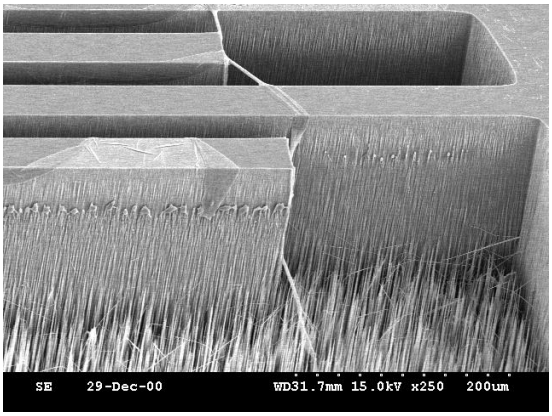

(c)

圖 3-4 (a)蝕刻效率大於保護效率，導致蝕刻結構底部形成外擴現象 (b)蝕刻效率小於保護效率，導致蝕刻結構底部形成內凹情形 (c)蝕刻結構側壁粗糙化及結構底部雜草現象

4. PoPLSE 製程平台：非等向性蝕刻

4.1. 製程壓力及 SF_6 蝕刻氣體流量之影響

非等向性蝕刻品質受到 ICP -RIE 各參數影響極大，不適當的參數，直接反應在蝕刻結構垂直度及形貌上，圖 4-1 為製程腔體壓力及蝕刻氣體 SF_6 流量對蝕刻形貌的影響，圖 4-2 為對應之蝕刻速率。其他參數為 A)蝕刻步驟：上/下電極 1000/12W，氣體流量 O_2 13 sccm，時間 12 sec，B)保護步驟：上/下電極 1000/0 W，氣體流量 C_4F_8 85 sccm，時間 8 sec，製程週期 60 cycle。製程腔體中的壓力越低，則電漿相互碰撞機率降低，基本上可獲得較佳的非等向性蝕刻，但腔體壓力越低，則真空度高，則會減少電漿濃度，使蝕刻速率變慢。在壓力 15 mTorr 及 SF_6 流量為 65 sccm 時，電漿離子濃度不足，導致結構底部出現雜草現象。另 SF_6 的流量越大，提供可蝕刻矽的氟離子濃度升高，使蝕刻速率提升；但在製程壓力 15 mTorr、SF_6 流量 195 sccm 時，因氣體流量太大導致製程無法穩定維持在 15 mTorr 而發生製程中斷情形。在 SF_6 流量為 130 sccm，不同製程壓力下，發現蝕刻結構底部形狀，由內凹轉變為外擴的情形，可知在不同製程壓力下會導致蝕刻與保護比例改變。由圖 4-2 所示，蝕刻速率隨蝕刻氣

體 SF_6 流量及製程壓力增大而增加。

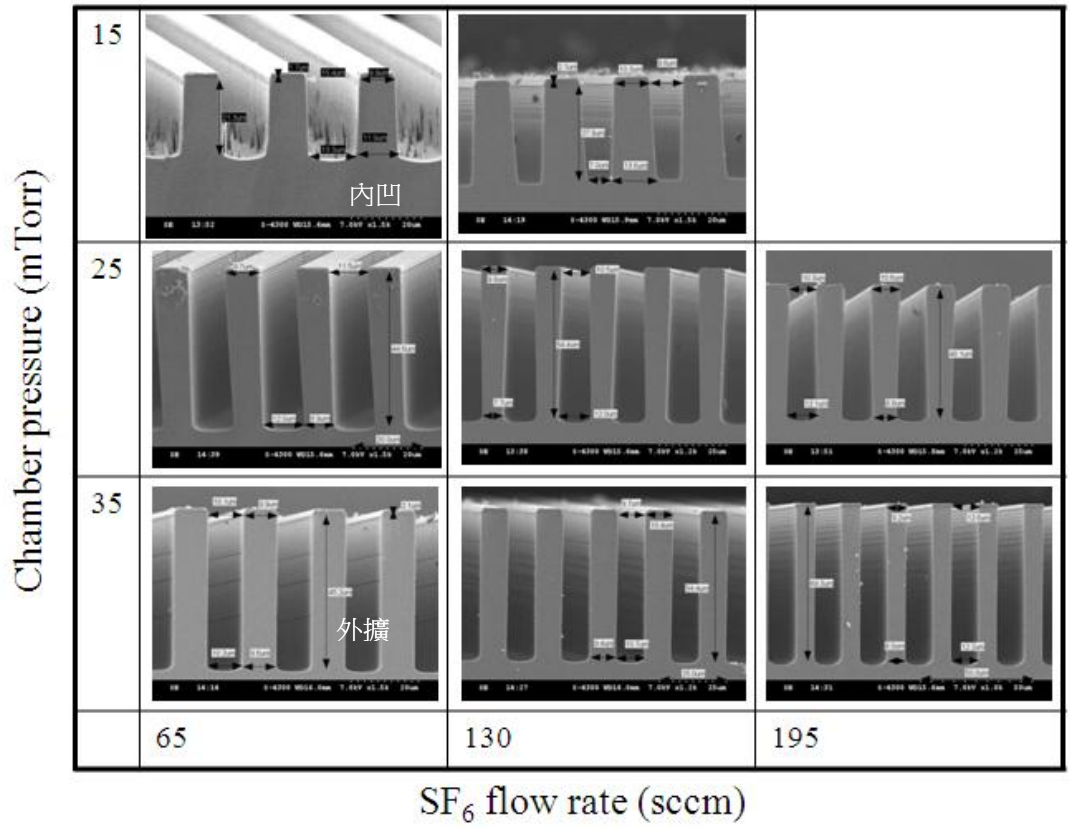

圖 4-1 製程腔體壓力及 SF_6 蝕刻氣體流量對蝕刻結構形貌的影響

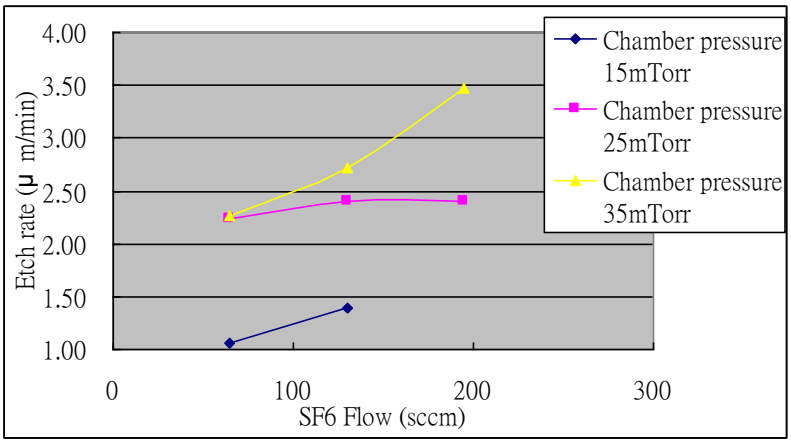

圖 4-2 製程腔體壓力及 SF_6 蝕刻氣體流量對蝕刻速率之關係圖

4.2. SF_6 蝕刻氣體流量及蝕刻時間之影響

蝕刻氣體 SF_6 流量及蝕刻時間對蝕刻形貌的影響如圖 4-3 所示，圖 4-4 為對應之蝕刻速率。其他參數為 A)蝕刻步驟：上/下電極 1000/12 W，氣體流量 O_2 13 sccm，B)保護步驟：上/下電極 1000/0 W，氣體流量 C_4F_8 85 sccm，時間 8 sec，製程腔體壓力 35 mTorr，製程週期 60 cycle。SF_6 流量增大，直接提供更多的蝕刻氟離子參與反應，因此，蝕刻速率提高，但由圖 4-4 中，SF_6 流量由 130 sccm 提高到 195 sccm 時，蝕刻速率增加並不多，其原因可能為反應之離子濃度已與蝕刻面積達飽和狀態。另在蝕刻時間 12 sec，SF_6 流量從 65 sccm 提高到 195 sccm 可發現，結構形貌由內凹轉變為外擴的現象，即為

蝕刻與保護的比例改變所致。

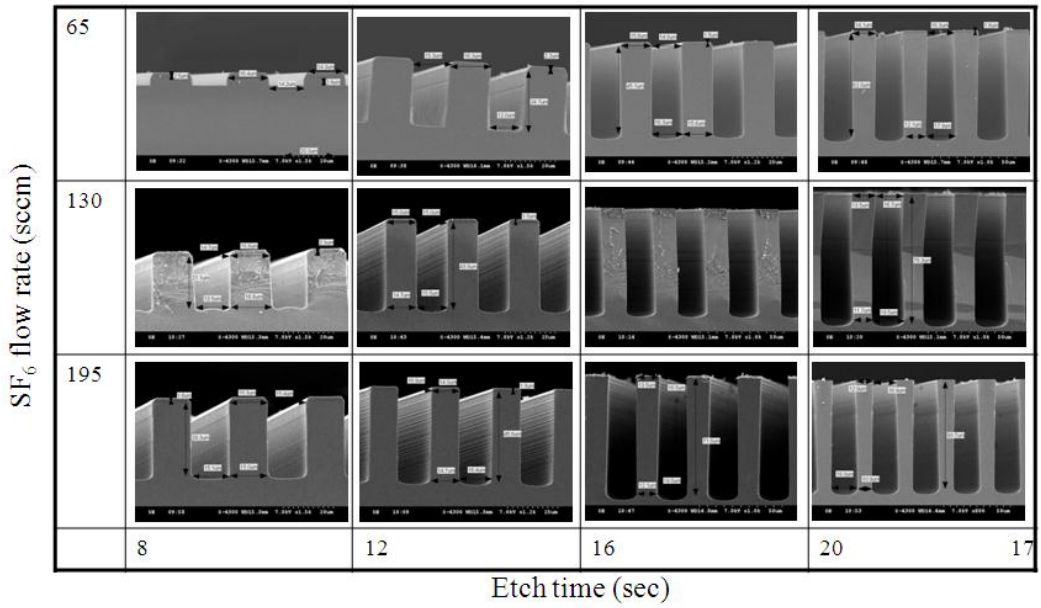

圖 4-3 SF_6 蝕刻氣體流量及蝕刻時間對蝕刻結構形貌的影響

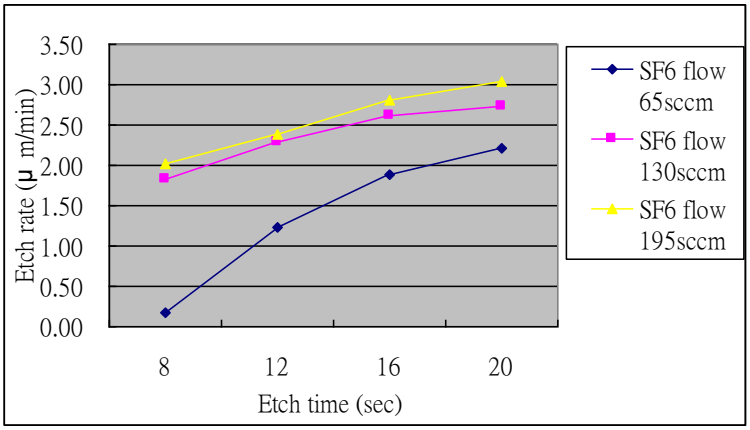

圖 4-4 SF_6 蝕刻氣體流量及蝕刻時間對蝕刻速率之關係圖

4.3. C_4F_8 保護氣體流量及保護時間之影響

圖 4-5 為不同流量保護氣體 C_4F_8 及保護時間對蝕刻形貌的影響，圖 4-6 為對應之蝕刻速率。其他參數為 A)蝕刻步驟：上/下電極 1000/12 W，氣體流量 SF_6/O_2 130/13 sccm，時間 12 sec，B)保護步驟：上/下電極 1000/0 W，製程腔體壓力 35 mTorr，製程週期 60 cycle。通入的保護氣體 C_4F_8 流量及時間增加下，底部鈍化膜增厚，需移除底部鈍化膜的時間增加，而降低了蝕刻速率。在保護氣體 C_4F_8 流量 85 sccm，保護時間由 4 sec 增加至 8 sec，明顯發現結構底部由外擴轉變為內凹情形，可見保護時間影響蝕刻結果極為敏感。另外保護氣體 C_4F_8 流量 60 sccm 時發現，結構偏上方形成碗狀的蝕刻缺陷，造成此原因為保護膜厚度不足，加上結構偏上方遭受到較多因光阻而改變行進方向的離子攻擊所導致[38]，需增加保護時間來提高保護膜厚度解決。

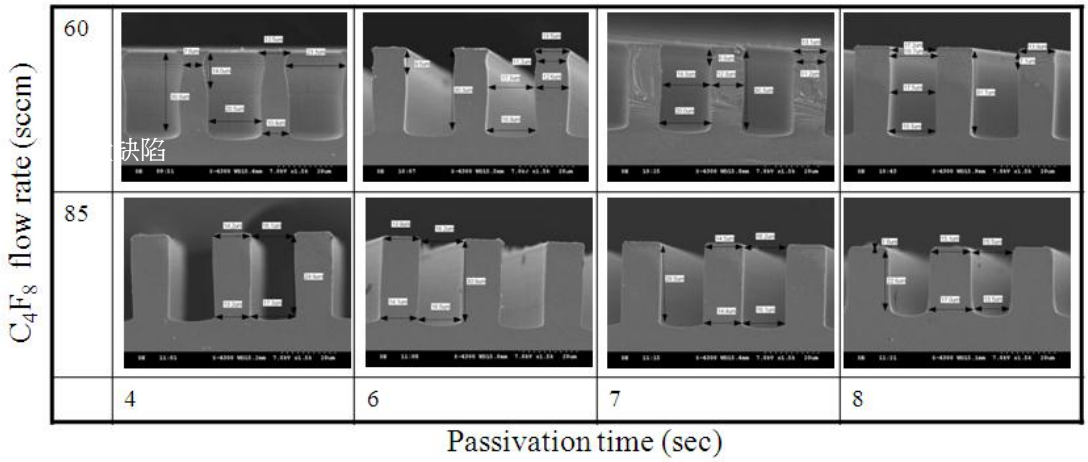

圖 4-5 C_4F_8 保護氣體流量及保護時間對蝕刻結構形貌的影響

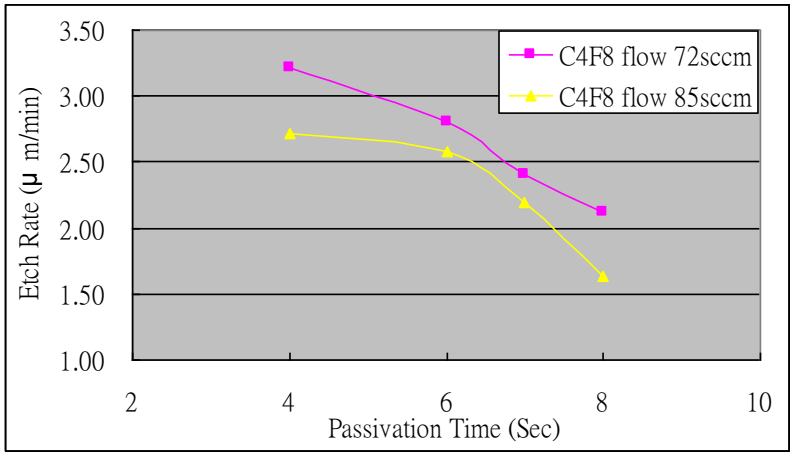

圖 4-6 C_4F_8 保護氣體流量及保護時間對蝕刻速率之關係圖

4.4. 上電極功率及保護時間之影響

圖 4-7 為上電極功率及保護時間對蝕刻形貌的影響，圖 4-8 為對應之蝕刻速率。其他參數為 A)蝕刻步驟：下電極 12W，氣體流量 SF_6/O_2 130/13sccm，時間 12sec，B)保護步驟：下電極 0W，氣體流量 C_4F_8 85 sccm，製程腔體壓力 35mTorr，製程週期 60 cycle。上電極為提供氣體解離能量，上電極功率越大，所解離出的離子濃度越高，在保護時間 8sec，上電極由 600W 提高到 1000W，發現結構偏上方出現側壁碗狀缺陷，同時蝕刻深度增加，表示，同樣參數條件下，上電極功率增大，對於蝕刻效果的影響大於保護效果。

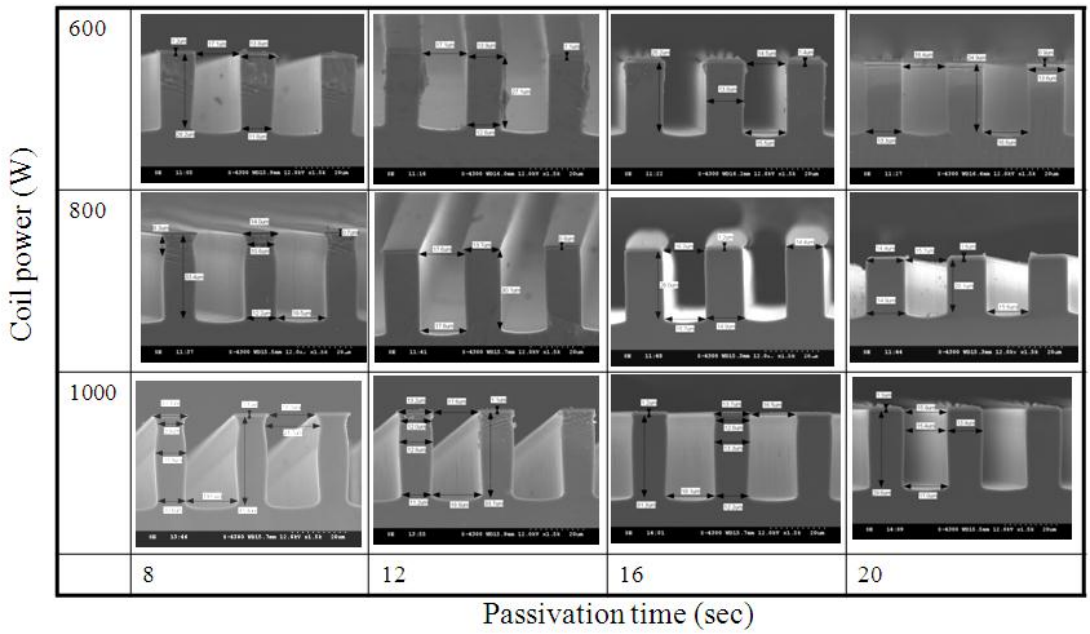

圖 4-7 上電極功率及保護時間對蝕刻結構形貌的影響

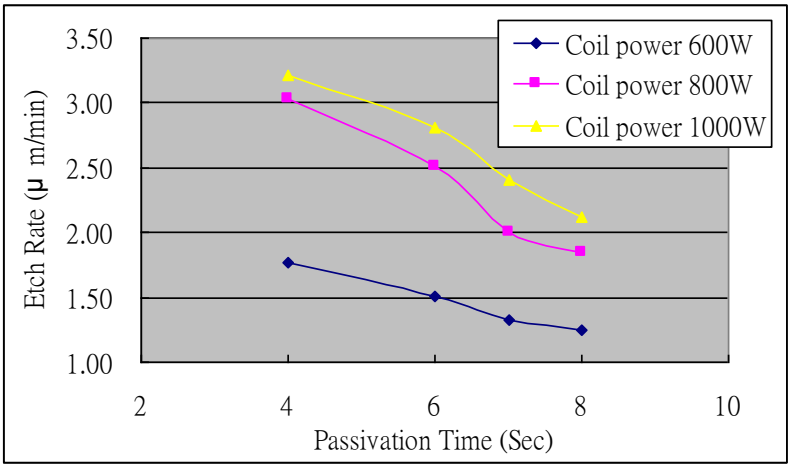

圖 4-8 上電極功率及保護時間對蝕刻速率之關係圖

4.5. 高深寬比蝕刻

高深寬比結構蝕刻除了需要蝕刻較深的結構深度外，保持結構的垂直度及確保結構幾何尺寸也相當重要，且整體製作的蝕刻速率也是外一項重要的考量因素，蝕刻速率太慢，則會影響蝕刻時間過長，產量過低而失去其意義。因此，提高蝕刻反應，調高蝕刻氣體流量及時間、上電極及下電極電壓，最後再調整適當相對之保護反應比例，獲得垂直度佳之蝕刻效果。

基於前述所建立的參數影響趨勢，調整出最佳化之蝕刻製程參數，獲得最佳之矽非等向性蝕刻參數為 A)蝕刻步驟：上/下電極 800/12 W，氣體流量 SF_6/O_2 130/13 sccm，時間 12 sec，B)保護步驟：上/下電極 800/0 W，氣體流量 C_4F_8 85 sccm，時間 8 sec，製程腔體壓力 35 mTorr，蝕刻速率在結構線寬 10 μm 處為 2.3 μm/min。以此參數蝕刻出之溝槽結構。如圖 4-9(a)所示，為結構線寬/開口尺寸 2 μm 的溝槽結構，蝕刻深度約 60 μm，深寬比為 30，垂直度 89±1°。圖 4-9(b)為結構線寬/開口尺寸 5 μm 的溝槽結構，蝕刻深度約 68 μm，深寬比為 15，垂直度為 89±1°。

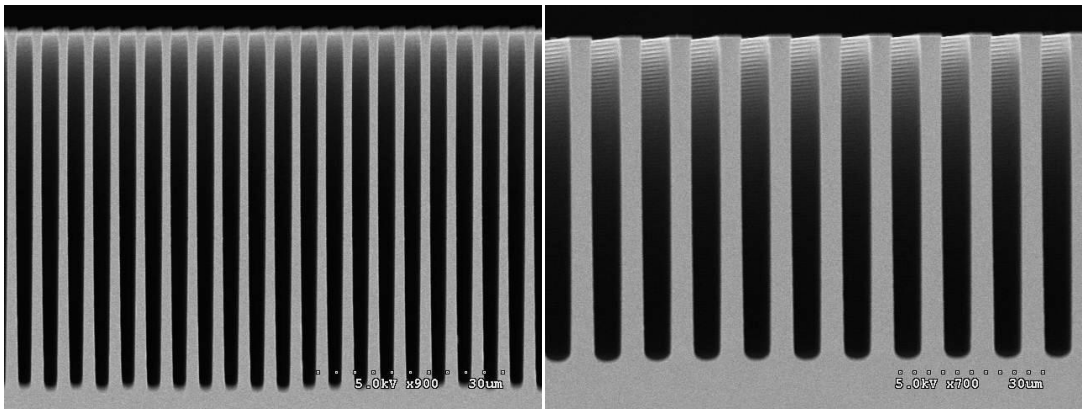

(a) (b)

圖 4-9 良好垂直度之非等向性蝕刻 (a)結構線寬/開口 2 μm 的溝槽結構，蝕刻深度約 60 μm，深寬比為 30 (b)結構線寬/開口 5 μm 的溝槽結構，蝕刻深度約 68 μm

以開發出之最佳高深寬比蝕刻參數進行蝕刻，並建立相對應之各項規格，圖 4-10 為溝槽結構線寬/開口尺寸為 2, 3, 4, 5, 6, 7, 8, 9, 10, 15, 20, 30, 40, 50 及 100 μm，蝕刻時間與蝕刻深度的關係，蝕刻深度越深時，因不同尺寸質傳效果不同的關係，導致蝕刻深度不一致，這即是蝕刻延遲的現象，在蝕刻 20 min 後，結構線寬/開口尺寸 2 μm 與 100 μm，蝕刻深度差異為 9 μm，在蝕刻 40 min 後，結構線寬/開口尺寸 2 μm 與 100 μm，蝕刻深度差異增為 25 μm，在蝕刻 160 min 後，結構線寬/開口尺寸 5 μm 以下的結構已不見，而結構線寬/開口尺寸 5 μm 與 100 μm，蝕刻深度差異高達為 195 μm，可見小線寬的尺寸，在蝕刻深度加深後，質傳效果遽增，導致蝕刻深度下降，蝕刻速率明顯降低。圖 4-11 為蝕刻時間與側蝕情形的關係圖，在蝕刻 40 min，側蝕小於 1.5 μm，而蝕刻 160 min 後，側蝕小於 3 μm。圖 4-12 為蝕刻時間與垂直度之關係圖，蝕刻 40 min ，垂直度為 89±1˚，在蝕刻 160 min ，垂直度為 87±1˚。在蝕刻側壁粗糙度上，以 AFM 進行量測，量測方式為取蝕刻深度之中間部份 10 μm×10 μm 範圍，結構線寬 10 μm 下，蝕刻時間與側壁粗糙度之關係圖，如圖 4-13 所示，蝕刻 20 min，側壁粗糙度為 18 nm(Ra)，蝕刻 40 min，側壁粗糙度為 73 nm(Ra)，蝕刻 160 min，側壁粗糙度為 145 nm(Ra)，蝕刻越深側壁粗糙度越差。

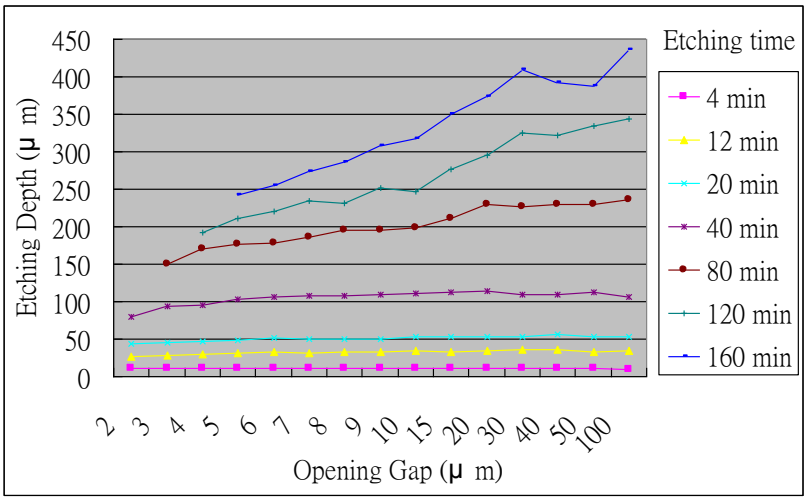

圖 4-10 不同蝕刻開口尺寸，蝕刻時間與蝕刻深度的關係圖

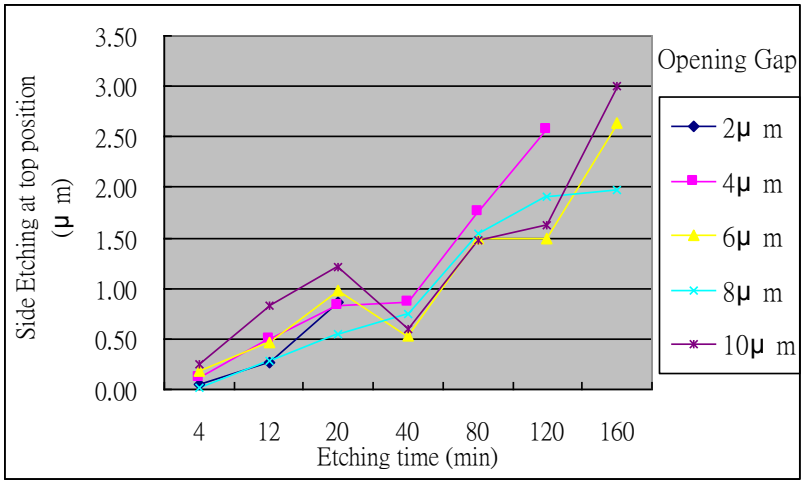

圖 4-11 不同開口尺寸下，蝕刻時間與側蝕關係圖

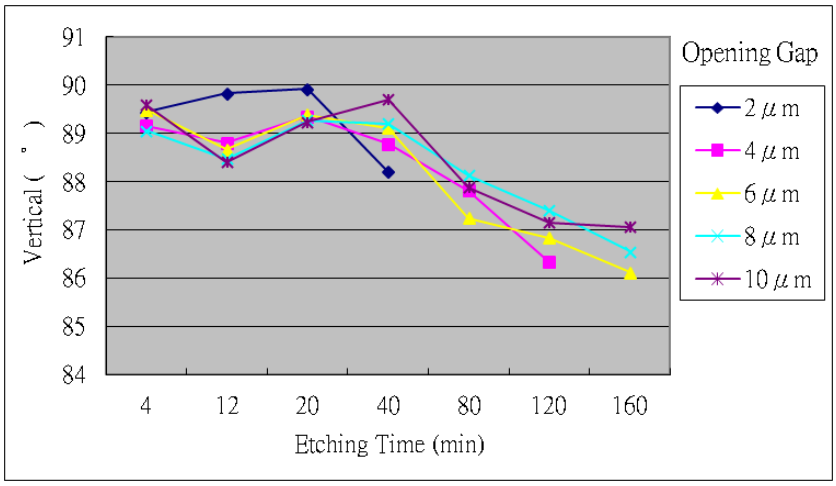

圖 4-12 不同開口尺寸下，蝕刻時間與垂直度關係圖

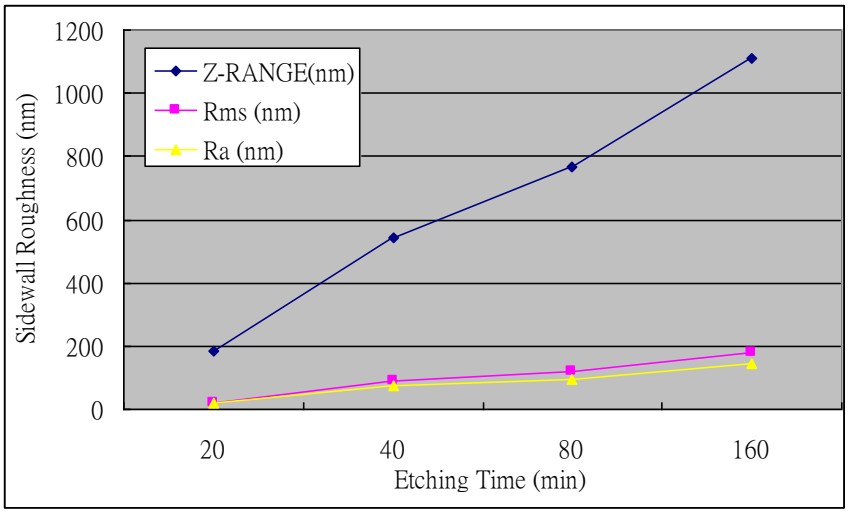

圖 4-13 側壁粗糙度與蝕刻時間之關係圖

5. PoPLSE 製程平台：等向性蝕刻

5.1. 高分子沈積及底部高分子去除

在 Bosch 專利蝕刻機制中，高分子是由 C_4F_8 氣體解離成電漿離子，進而沈積成高分子薄膜，電漿離子是由 CF_x^+、CF_x^*和 F^*等化合物組成，*CFx**化合物經 由吸附作用，在矽結構表面形成高分子薄膜，藉由這層 CF_2 薄膜來阻擋氟離子蝕刻矽質材料。高分子材料經由 Hitachi S-4300 場發射掃瞄電子顯微鏡中 EDS，進行高分子薄膜成分分析，如圖 5-1 所示，高分子成份由 45%的碳及 55%的氟組成。待測之高分子為厚度 500 nm 沈積於矽基板上，高分子沈積參數為上/下電極 800/0W，C_4F_8 氣體流量 130 sccm，製程腔體壓力 35 mTorr，時間 5 min，EDS 之加速電壓為 15 kv，$1x10^{-5}$ Pa 真空度。

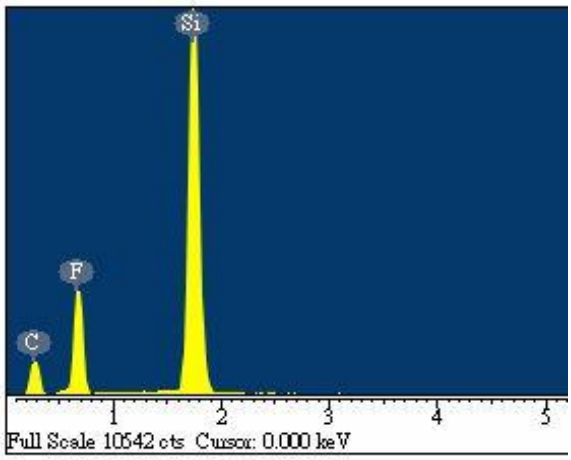

圖 5-1 高分子薄膜 EDS 成分分析

在 Bosch 蝕刻保護交替機制來獲得高深寬比蝕刻中，產生的側壁波紋結構會影響高分子沈積覆蓋的結果，波紋結構會對高分子進行沈積時，產生遮蔽的影響，使得在波紋結構下方，高分子薄膜不容

易覆蓋好，在等向性蝕刻時，容易對高分子覆蓋有缺陷的地方，產生矽結構蝕刻現象，因此，對於高分子在側壁波紋結構及不同開口尺寸下的覆蓋效果，先進行研究。

利用 Bosch 非等向性標準高深寬比蝕刻參數，蝕刻出深度 30 μm 的溝槽結構，溝槽開口尺寸分別為 5、10、30 及 50 μm，高分子沈積時間 5, 10, 15 及 25 min，來探討高分子沈積及底部高分子移除的情形。

在高分子沈積過程中，不提供下電極靜電偏壓，讓高分子利用擴散方式，等向性的覆蓋在矽結構的表面，在不同開口尺寸及沈積時間下，高分子薄膜沈積在溝槽結構側壁之 SEM，所圖 5-2 所示，高分子薄膜沈積在溝槽結構底部之 SEM，所圖 5-3 所示。

在不同沈積條件下，以 SEM 量測高分子沈積在結構表面的厚度，如圖 5-4 所示，高分子是用來作為製作懸浮結構製程中，抵擋等向性蝕刻之保護矽結構材料，必須確保矽結構的側壁完全被高分子包覆，因此，側壁所沈積的高分子厚度，量測其最小值，圖 5-4(a)為高分子沈積在矽結構側壁量測之最小厚度值，最小厚度發現在結構偏下方處，因質傳效果影響所致。在相同高分子沈積時間下，沈積在開口尺寸小的高分子薄膜的厚度小於沈積在開口尺寸大的。在開口尺寸 5 μm 及 10 μm 處，由於側壁波紋結構的遮蔽效果，導致波紋結構下方沈積較薄的高分子薄膜，加上沈積時間短如 5 min 時，發現在某些波紋結構下方，沒有高分子薄膜沈積，厚度量測值為 0，將高分子沈積時間由 5 min 增加至 25 min 來增加沈積的高分子薄膜厚度，在波紋結構下方的高分子薄膜厚度，依然遠薄於沈積在其他結構的區域。為改善在開口尺寸小，因波紋結構遮蔽效應導致高分子薄膜沈積覆蓋性差的問題，可以調整非等向性蝕刻的參數，降低側壁波紋結構及粗糙度，如本論文 3.2.2 節所述，側壁鏡面蝕刻可有效改善因波紋導致高分子覆蓋差的情形。在開口尺寸 30 μm 及 50 μm 時，側壁波紋結構之遮蔽效果影響變小，高分子薄膜能較均勻地沈積在側壁表面。

由於在製作懸浮結構製程中，底部高分子薄膜需要完全去除，以利後續的等向性蝕刻的進行，因此，沈積在結構底部高分子薄膜厚度，量測其最大值，如圖 5-4(b)所示，沈積在結構底部高分子薄膜的厚度，隨著開口尺寸及沈積時間的增加而增厚。底部高分子薄膜移除之非等向性蝕刻參數為上/下電極 800/12 W，氣體 SF_6/O_2 130/13 sccm，製程腔體壓力 35 mTorr，在溝槽結構深度 30 μm 及四種不同開口尺寸下，因質傳效果，開口尺寸較大處有較高的高分子薄膜移除速率，如圖 5-5 所示。

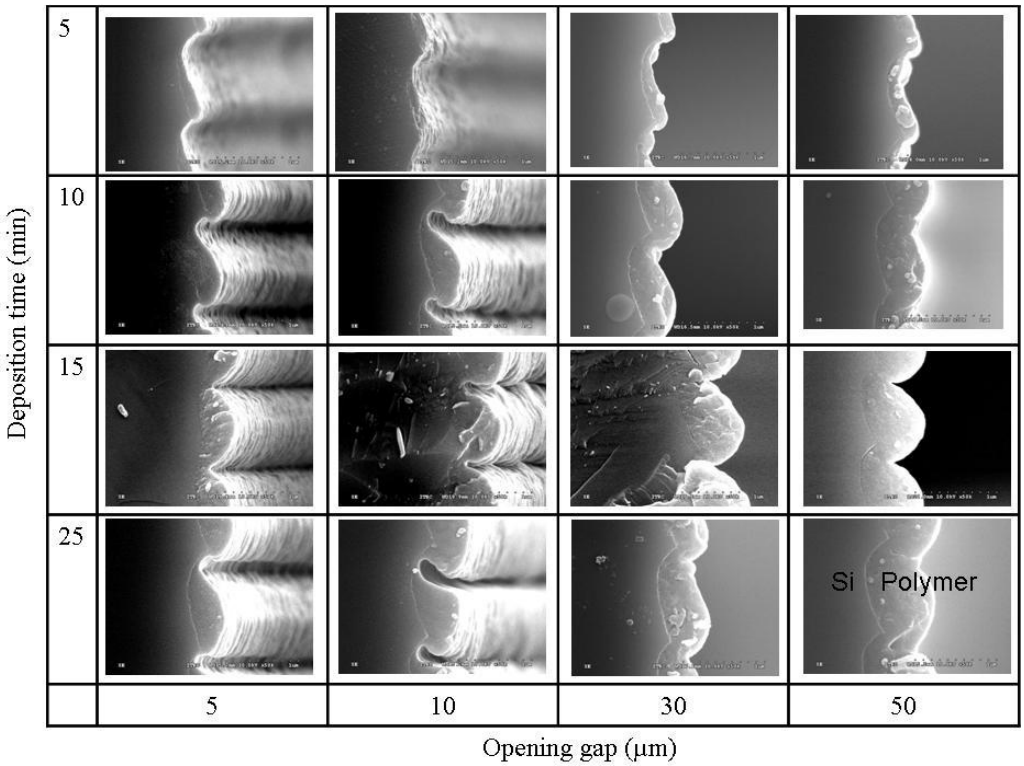

圖 5-2 高分子薄膜沈積在溝槽結構側壁之 SEM 圖，溝槽結構深度為 30 μm，開口尺寸為 5、10、30、50 μm 及高分子沈積時間 5、10、15、25 分鐘

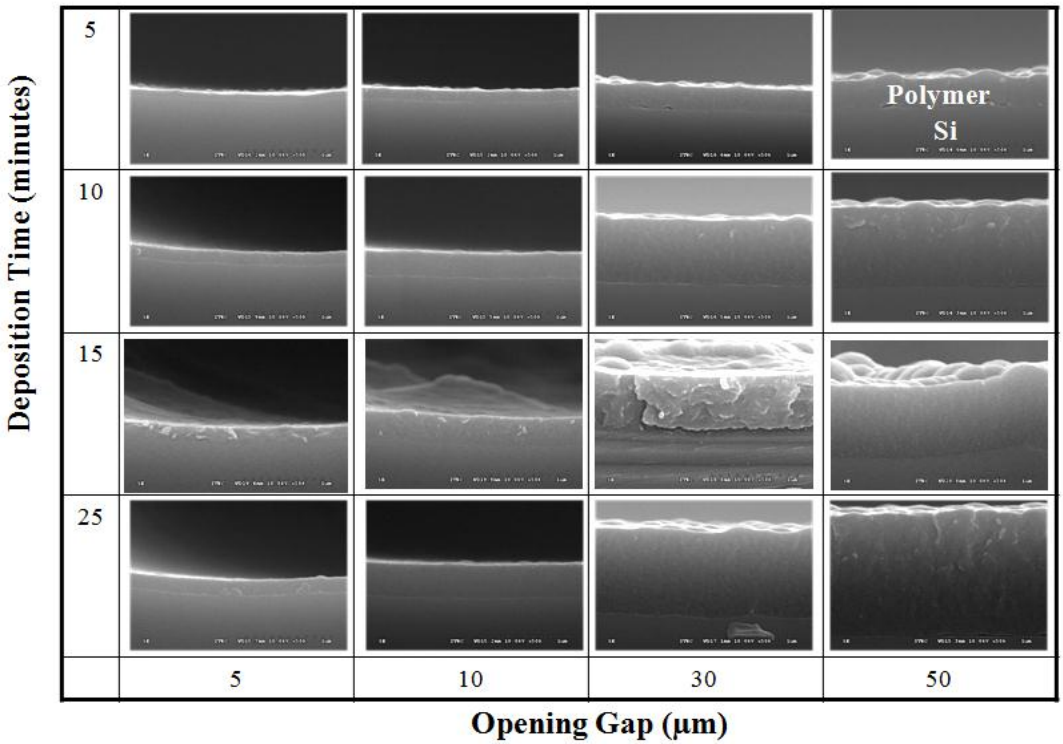

圖 5-3 高分子薄膜沈積在溝槽底部之 SEM 圖，溝槽結構深度為 30 μm，開口尺寸為 5、10、30、50 μm 及高分子沈積時間 5、10、15、25 分鐘

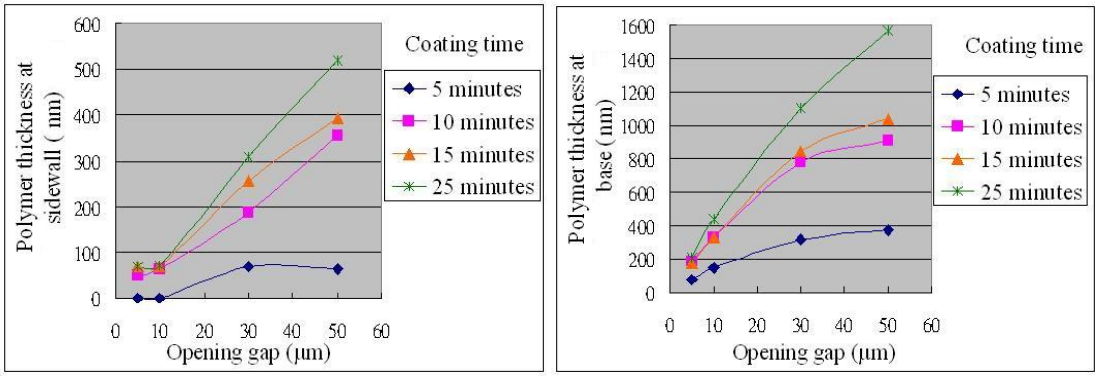

(a) (b)

圖 5-4 在不同開口尺寸及沈積時間下，溝槽結構 30 μm 之高分子薄膜厚度量測 (a) 側壁高分子量測厚度最小值 (b)結構底部高分子量測厚度最大值

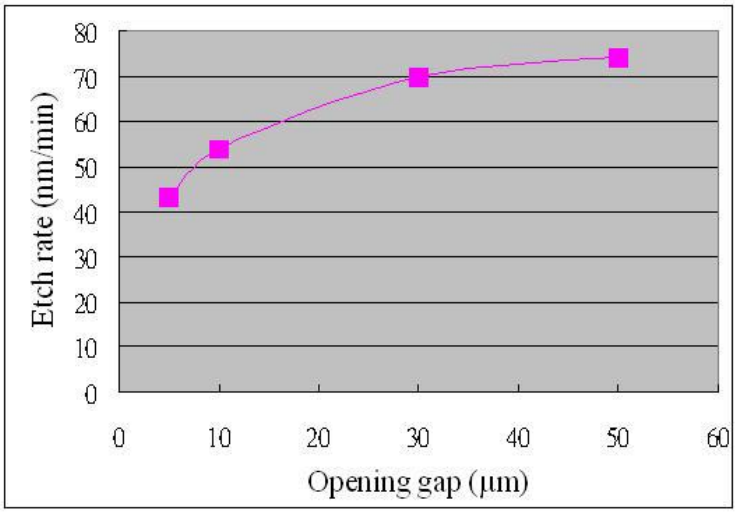

圖 5-5 不同開口尺寸下，結構 30 μm 底部高分子移除速率

5.2. 結構深度 30 μm 之等向性蝕刻

利用等向性蝕刻將懸浮結構底部之矽材料移除，及等向性蝕刻之側蝕情形、蝕刻速率與結構開口尺寸及結構深度有關，本實驗預先蝕刻出結構深度 30μm 開口尺寸分別為 5μm、10μm、30μm、50 μm 後，進行高分子保護層之沉積後再使用非等向性蝕刻轟擊將結構底部所沉積之高分子保護層去除只留下側壁高分子保護層後開始等向性蝕刻，等向性蝕刻後發現底部未受高分子保護層之矽基材越靠近原始結構底部之位置開口越大，因等向性蝕刻呈現出碗狀形狀，因離子往每個方向蝕刻之機率較相同所致，離子反應未受阻，蝕刻速率較快，開口尺寸越小及結構深度越深時，受限於光阻及矽結構影響，蝕刻離子需行經光阻結構及矽結構深度，才能到達底部矽表面產生蝕刻反應，如圖 5-6 所示，因此蝕刻速率下降，同時蝕刻形狀並非呈碗狀，而呈現似菱形的蝕刻形狀，開口尺寸越小，側蝕蝕刻速率越慢，蝕刻形狀越趨菱形，其參數為高分子沈積時間為 10 分鐘，底部高分子移除時間為 8 分鐘及等向性蝕刻時間為 6 分鐘。

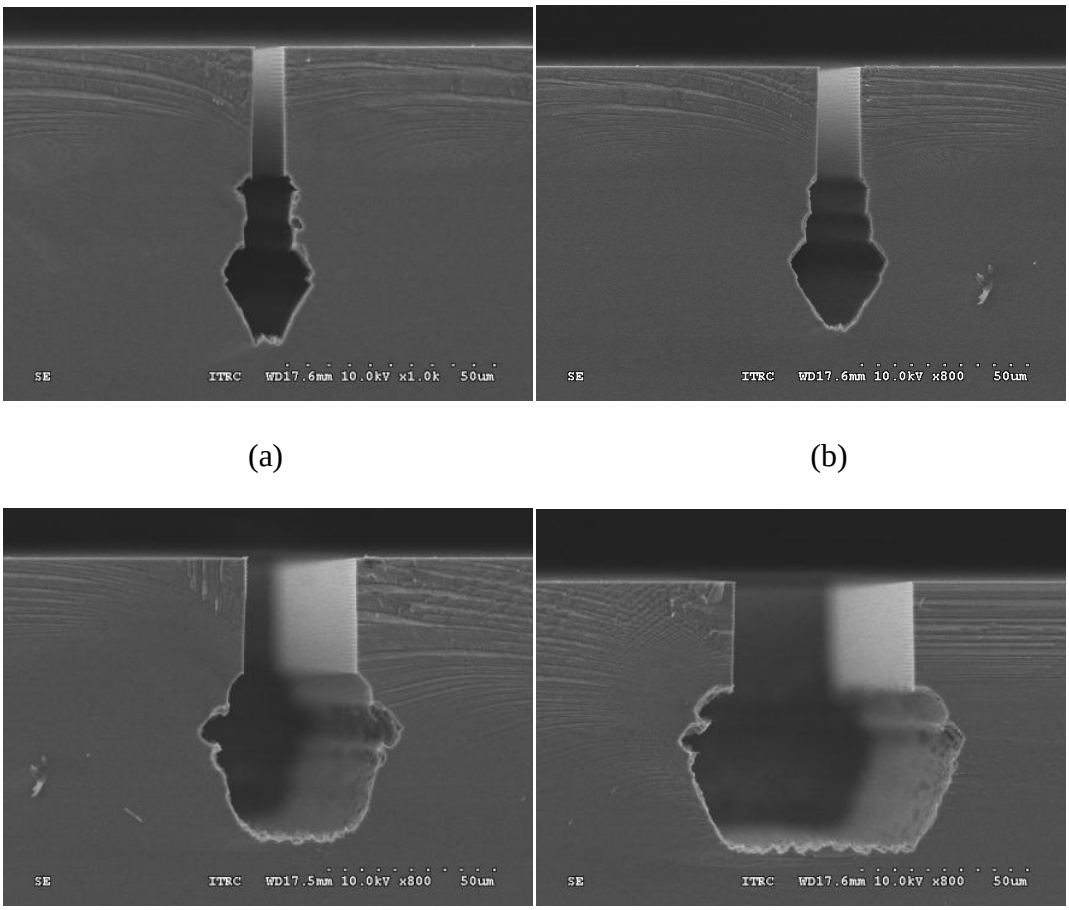

(a) (b)

(c) (d)

圖 5-6 結構深度 30 μm，不同開口尺寸(a)5 (b)10 (c)30 (d)50 μm 之等向性蝕刻結果

5.3. 懸浮結構製程結果

基於優化的參數研究，於結構厚度 30 μm 及結構線寬/開口尺寸 5 μm 之單晶矽懸浮結構，在高分子沈積時間為 10 分鐘、底部高分子去除時間為 8 分鐘及等向性蝕刻時間為 6 分鐘的參數下，可以成功製作出來。因為 PoPLSE 製程平台製作懸浮結構在同一片單晶矽晶片上，除懸浮結構處外，需有支撐結構處，因此支撐結構處的尺寸需大於懸浮結構處，如圖 5-7 所示，利用尺寸的差異性，控制好懸浮蝕刻的時間，來決定懸浮的結構。圖 5-8(a)為利用 PoPLSE 製程平台技術製作之結構深度 30 μm，結構線寬 5 μm 之梳狀致動器，圖 5-8(b)為側向放大圖，可明顯看出懸浮微結構側壁被保護而底部懸浮掏空的結果。各種微感測器如微陀螺儀、微電容感測器、扭轉式梳狀致動器及微鑷子致動器等，都能利用所提出之 PoPLSE 製程平台製程技術製作，如圖 5-9。

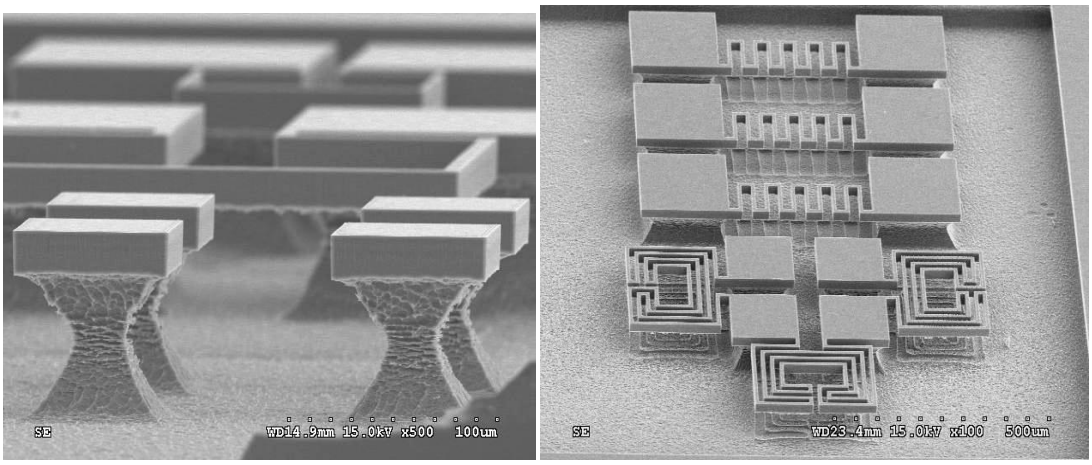

(a) (b)

圖 5-7 利用線寬尺寸的差異，懸浮與未懸浮的結構

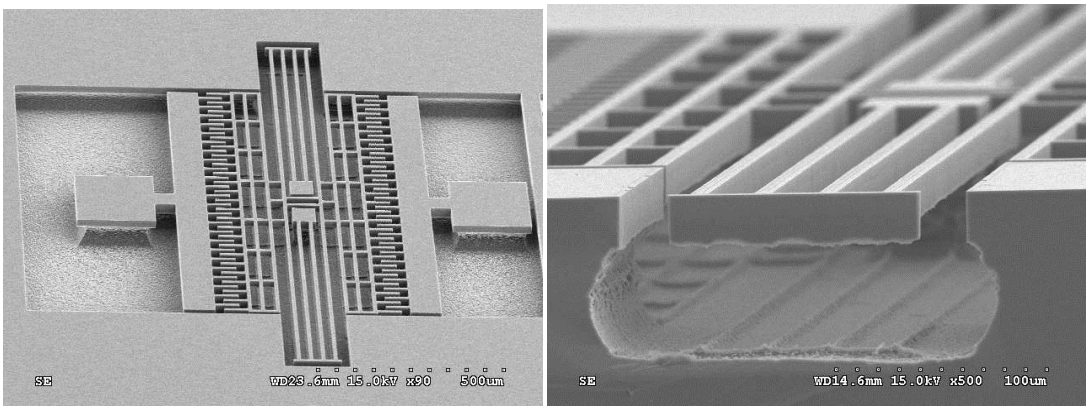

(a) (b)

圖 5-8 結構深度 30 μm、結構寬度 5 μm (a)懸浮梳狀致動器結構圖 (b)彈簧結構懸浮放大圖

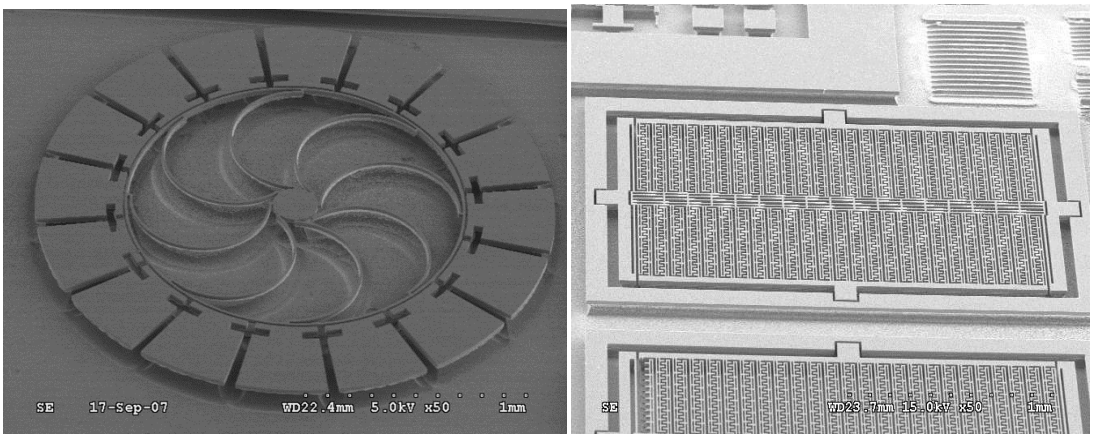

(a) (b)

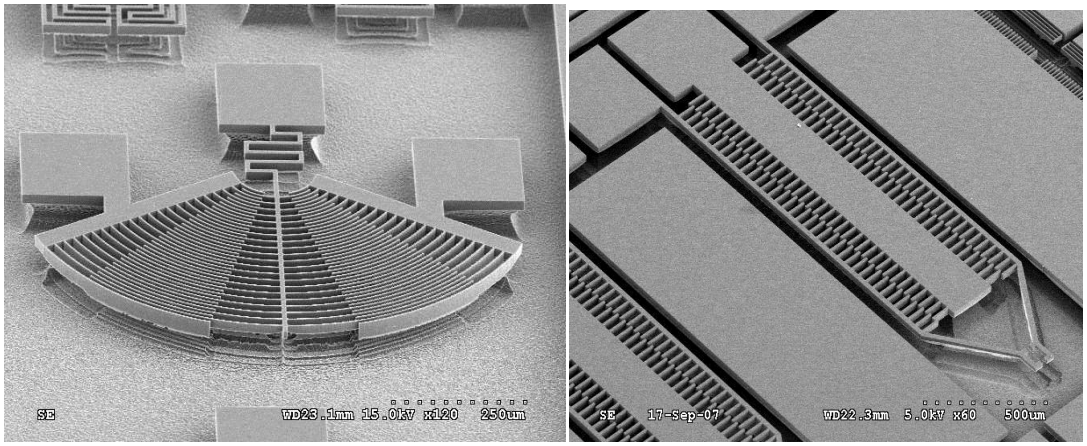

(c) (d)

圖 5-9 PoPLSE 製程平台技術製作出各式厚度 30 μm 之微結構 (a)微陀螺儀 (b)微電容感測器 (c)扭轉式梳狀致動器 (d)微鑷子致動器

懸浮結構結構線寬增加時，除等向性蝕刻時間隨之增加，其高分子沈積及底部高分子移除的參數也需隨之調整。以結構深度 30 μm、結構寬度 10 μm 之梳狀結構來討論適合的參數，圖 5-10(a)為高分子沈積時間 10 分鐘、底部高分子移除時間 8 分鐘，等向行蝕刻時間 9 分鐘，所製作之懸浮梳狀結構。靠近結構下方依然有因高分子沒保護好微結構，而導致被蝕刻的結構缺陷。增加高分子沈積時間到 15 分鐘、底部高分子移除時間隨之調整至 10 分鐘，等向性蝕刻時間維持 9 分鐘，可以成功製作出結構寬度 10 μm、結構深度 30 μm 之懸浮梳狀結構，如圖 5-10(b)所示。

當結構深度增加，結構越深高分子越不容易沈積，因此沈積時間得增長，同時底部高分子移除及等向性蝕刻參數也需隨之調整。圖 5-11 為利用 PoPLSE 製程平台技術，成功製作結構深度 60 μm，結構寬度各為 5 μm 及 10 μm 之梳狀懸浮微結構，製程參數為高分子沈積時間 25 分鐘，底部高分子移除時間 14 分鐘及等向性蝕刻時間 9 分鐘。

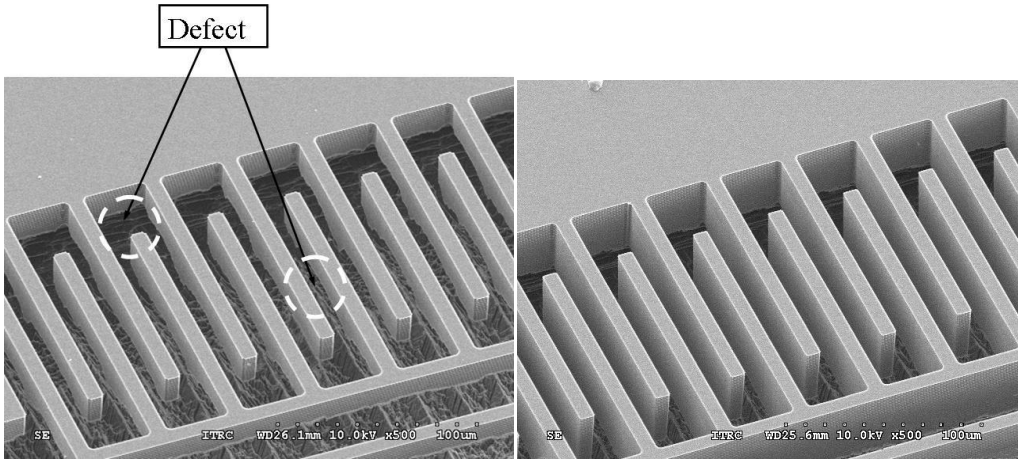

(a) (b)

圖 5-10 結構線寬/開口尺寸 10 μm、結構深度 30 μm 之懸浮梳狀結構 (a)因不足的高分子保護導致結構缺陷（高分子沈積 10 分鐘、底部高分子移除 8 分鐘及等向性蝕刻 9 分鐘）(b)成功製作之梳狀結構（高分子沈積 15 分鐘、底部高分子移除 10 分鐘及等向性蝕刻 9 分鐘）

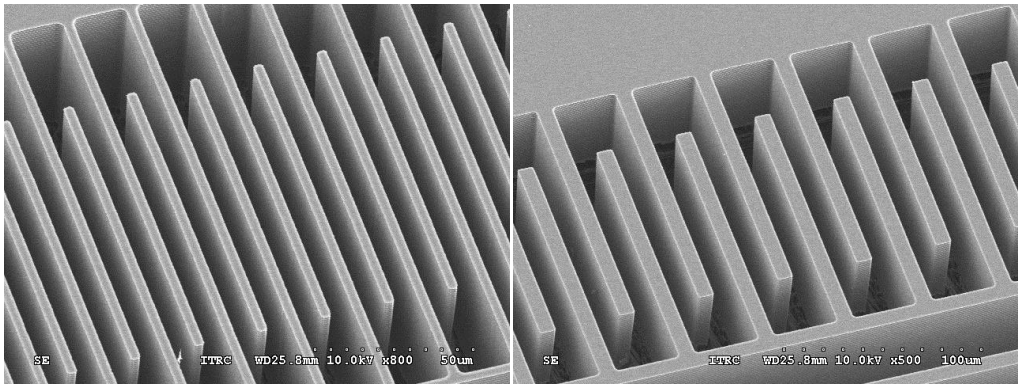

(a) (b)

圖 5-11 成功製作之梳狀結構，結構深度 60 μm，結構線寬/開口尺寸 (a)5 μm (b) 10 μm

6. 結論

PoPLSE 製程之各項參數對於元件製作皆有相當大的影響，進行非等向性蝕刻主要以製程壓力、SF_6 蝕刻氣體流量、蝕刻時間、C_4F_8 保護氣體流量、保護時間及上電極功率為主要影響因素，而針對各參數進行優化進而得到高深寬比、結構垂直性佳及較佳的側壁粗糙度。於等向性蝕刻製程中主要影響參數為高分子沉積時間、高分子層去除時間及等向性蝕刻時間，本研究以深度 30 μm 之溝槽結構於開口尺寸 5、10、30 及 50 μm 進行測試，觀察側壁高分子沈積及底部高分子去除於不同開口尺寸下之趨勢。並探討在不同結構線寬、開口尺寸及結構深度等條件下，底部高分子移除及等向性懸浮對高分子保護膜之影響，並且得到優化參數成功釋放梳狀結構以驗證 PoPLSE 製程平台製作懸浮結構可行性。PoPLSE 製程平台技術利用高分子作為蝕刻保護層來製作懸浮結構，可簡化製程機台、縮短製程時間、降低製程晶片成本及應用共通性廣等為此 PoPLSE 製程平台的優勢。

7. 參考資料

[1] K. E. Peterson, Silicon as a mechanical material, *Proc. IEEE*, vol.70, no. 5, pp. 420-457, 1982

[2] http://www.jahm.com/：Temperature Dependent Elastic & Thermal Properties Database

[3] G. T. A. Kovacs, N. I. Maluf and K. E. Petersen, Bulk micromachining of silicon, *Proc. IEEE*, vol. 86, no. 8, 1998

[4] H. R. Robbins and B. Schwartz, Chemical etching of silicon-I. The system HF, HNO_3 H_2O and $HC_2C_3O_2$, *Journal of The Electrochemical Society*, vol. 106, no. 6, pp. 505–508, 1959

[5] H. R. Robbins and B. Schwartz, Chemical etching of silicon-II. The system HF,HNO_3 H_2O and $HC_2C_3O_2$, *Journal of The Electrochemical Society*, vol. 107, no. 2, pp. 108–111, 1960

[6] B. Schwartz and H. R. Robbins, Chemical etching of silicon-III. A temperature study in the acid system, *Journal of The Electrochemical Society*, vol. 108, no. 4, pp. 365–372, 1961

[7] J. B. Price, Anisotropic etching of silicon with KOH-H_2O isopropyl alcohol, *in Semiconductor Silicon, H. R. Huff and R. R. Burgess, Eds. Princeton, NJ: Electrochemical Society*, pp. 339-353, 1973

[8] B. Schwartz and H. R. Robbins, Chemical etching of silicon-IV. Etching technology, *Journal of The Electrochemical Society*, vol. 123, no. 12, pp. 1903–1909, 1976

[9] E. Bassous, Fabrication of novel three-dimensional microstructures by the anisotropic etching of (100) and (110) silicon, *IEEE Trans. Electron Devices*, vol. ED-25, pp. 1178–1185, 1978

[10] H. Seidel, L. Csepregi, A. Heuberger and H. Baumgartel, Anisotropic etching of crystalline silicon in alkaline solutions I: Orientation dependence and behavior of passivation layers, *Journal of The Electrochemical Society*, vol.137, no.11, pp. 3612–3626, 1990

[11] H. Seidel, L. Csepregi, A. Heuberger and H. Baumgartel, Anisotropic etching of crystalline silicon in alkaline solutions II: Influence of dopants, *Journal of The Electrochemical Society*, vol. 137, no. 11, pp. 3626–3632, 1990

[12] F. S. S. Chien, C. L. Wu, Y. C. Chou, T. T. Chen, S. Gwo and W. F. Hsieh, Nanomachining of 110-oriented silicon by scanning probe lithography and anisotropic wet etching, *Applied Physics Letters*, vol. 75, no. 16, pp. 2429-2431, 1999

[13] X. Li and P. W. Bohn, Metal-assisted chemical etching in HF/H_2O_2 produces porous silicon, *Applied Physics Letters*, vol. 77, no. 16, pp. 2572-2574, 2000

[14] T. Hadjersi, N. Gabouze, N. Yamamoto, C. Benazzouz, H. Cheraga, Blue luminescence from porous layers produced by metal-assisted chemical etching on low-doped silicon, *Vacuum*, vol. 80, pp. 366–370, 2005

[15] K. Peng, J. Hu, Y. Yan, Y. Wu, H. Fang, Y. Xu, S. Lee and J. Zhu, Fabrication of single-crystalline silicon nanowires by scratching a silicon surface with catalytic metal particles, *Advanced Functional Materials*, vol. 16, pp. 387–394, 2006

[16] C. Chartier, S. Bastide and C. L. Clement, Metal-assisted chemical etching of silicon in HF-H_2O_2, *Electrochimica Acta*, vol. 53, pp. 5509–5516, 2008

[17] F. Chamran, Y. Yeh, B. Dunn and C. J. Kim, 3-Dimensional electrodes for microbatteries, *ASME Conf. Proc.*, IMECE2004-61925, pp. 289-292, 2004

[18] L. M. Ephrath, Reactive Ion Etching, *US Patent* 4283249, 1979

[19] S. A. McAuley, H. Ashraf, L. Atabo, A. Chambers, S. Hall, J. Hopkins and G. Nicholls, Silicon micromachining using a high-density plasma source, *Journal of Physics D: Applied Physics.*, vol. 34, pp. 2769–2774, 2001

[20] F. Larmer and A. Schilp, Method of anisotropically etching silicon, *US patent* 5501893, 1996

[21] A. M. Hynes, H. Ashraf, J. K. Bhardwaj, J. Hopkins, I. Johnsto and J. N. Shepherd, Recent advantages in silicon etching for MEMS using the ASE^{TM} process, *Sensors and Actuators A*, vol. 74, pp. 13-17, 1999

[22] F. Laermer, A. Schilp, K. Funk and M. Offenberg, Bosch deep silicon etching: improving uniformity and etch rate for advanced mems applications, *Proc. IEEE*, pp. 211-216, 1999

[23] J. B. Lasky, Wafer bonding for silicon−on−insulator technologies, *Applied Physics Letters*, vol. 48, pp. 78-80, 1986

[24] M. Bruel, Silicon on insulator material technology, *Electronics Letters*, vol. 31, no.14, pp. 1201-1202, 1995

[25] S. C. Arney and N. C. MacDonald, Formation of submicron silicon on insulator structures by lateral oxidation of substrate-silicon islands, *Journal of Vacuum Science & Technology B*, vol. 6, pp. 341-345, 1998

[26] W. H. Juan and S. W. Pang, Released Si microstructures fabricated by deep etching and shallow diffusion, *Journal of Microelectromechanical Systems*, vol. 5, pp. 18-23, 1996

[27] C. G. Keller and R. T. Howe, HEXSIL tweezers for teleoperated micro-assembly, *Proc. IEEE*, pp. 72-77, 1997

[28] F. Ayazi and K. Najafi, High aspect-ratio combined poly and single crystal silicon (HARPSS) MEMS technology, *Journal of Microelectromechanical Systems*, vol. 9, pp. 288-294, 2000

[29] K. A. Shaw, Z. L. Zhang and N. C. MacDonald, SCREAM I: A Single Mask, Single-Crystal Silicon, Reactive Ion Etching Process for MicroElectroMechanical Structures, S*ensors and Actuators A*, vol. 40, pp. 63-70, 1994

[30] N. C. MacDonaid, SCREAM microelectromechanical systems, *Microelectronic Engineering*, vol. 32, pp. 49-73, 1996

[31] S. Lee; S. Park, J. Kim, S. Lee and D. Cho, Surface/bulk micromachined single-crystalline-silicon micro-gyroscope, *Journal of Microelectromechanical Systems*, vol. 9, pp. 557-567, 2000

[32] J. Hsieh and W. Fang, A boron etch stop assisted lateral silicon etching process for improved high aspect ratio silicon micromachining and its applications, *Journal of Micromechanics and Microengineering*, vol.12, pp. 574-581, 2002

[33] J. M. L. Tsai, H. Y. Chu, J. Hsieh and W. Fang, The BELST II process for silicon HARM vertical comb actuator and its applications, *Journal of Micromechanics and Microengineering*, vol. 14, pp. 235-241, 2004

[34] H. Jansen, M. de Boer, R. Wiegerink, N. Tas, E. Smulders, C. Neagu and M. Elwenspoek, RIE lag in high aspect ratio trench etching of silicon, *Microelectronic Engineering*, vol. 35, Issues 1–4, pp. 45–50, 1997

[35] S. L. Lai, D. Johnson and R. Westerman, Aspect ratio dependent etching lag reduction in deep silicon etch processes, *Journal of Vacuum Science & Technology A*, vol. 24, no. 4, pp. 1283-1288, 2006

[36] J. Li, Q. X. Zhang, A. Q. Liu, W. L. Goh and J. Ahn, Technique for preventing stiction and notching effect on silicon-on-insulator microstructure, *Journal of Vacuum Science & Technology B*, vol. **21**, pp. 2530-2539, 2003

[37] S. Park, D. Kwak, H. Ko, T. Song and D. Cho, Selective silicon-on-insulator (SOI) implant: a new micromachining method without footing and residual stress, *Journal of Micromechanics and Microengineering*, vol. 15, pp. 1607–1613, 2005

[38] G. Marcos, A. Rhallabi and P. Ranson, Monte Carlo simulation method for etching of deep trenches in Si by a SF_6/O_2 plasma mixture, *Journal of Vacuum Science & Technology A*, vol. 21, no. 1, pp.87-95, 2003

國科會補助專題研究計畫出席國際學術會議心得報告

日期：101 年 07 月 31 日

計畫編號	NSC　100－2221－E－009－034－		
計畫名稱	以高分子作為感應偶合電漿反應離子蝕刻側壁保護以製作單晶矽懸浮微結構之快速製程平台研發		
出國人員姓名	徐文祥、卓琮閔	服務機構及職稱	交通大學機械系教授、研究生
會議時間	2012 年 03 月 05 日 至 2012 年 03 月 08 日	會議地點	日本，京都
會議名稱	(中文)奈米/微米工程與分子系統國際研討會 (英文)2012 7th IEEE International Conference on Nano/Micro Engineered and Molecular Systems		
發表題目	共兩篇 Development of Microbead-based Affinity Biosensor by Insulator-Based Dielectrophoresis Fabrication of Deep Lateral Single-Crystal-Silicon Blaze Micro-grating by Inductively-Coupled-Plasma Reactive Ion Etch		

一、參加會議經過

IEEE NEMS Conference 是一有關微工程技術交流之國際研討會，其領域包括生醫感測器、半導體製程及最新的生物領域相關技術，每年度於世界各地舉辦一次，與會人士皆為世界各地之頂尖學者及研究人員；今年會議日期為 2012/3/5 至 2012/3/8 共四天，主辦單位為京都大學，會議則於日本的京都舉行，京都有悠久歷史為日本獲選世界遺產的城市之一，其建築群主要效仿隋唐長安城與洛陽城設計古稱平安京，於桓武天皇時期完成(西元 794 年)定為國都直到明治天皇(西元 1868 年)遷都東京為止，為日本歷經千年的政治及文化的中心。

第一天主要於京都大學內辦理報到相關事宜，參加者領取名牌及會議相關資料。第二天至第四天則為正式議程，包含每日九點開始的例行的研討會議，每日會議歷程分上午與下午共有四個場次，此外除每日例行研討會議也於午後時段舉行海報報告，讓與會者皆能找到感興趣之研究主題，此次會議共計有 230 場的口頭報告與 104 場的海報報告。

本實驗室在此會議共發表兩篇論文，其中”Development of Microbead-based Affinity Biosensor by Insulator-Based Dielectrophoresis”是安排為口頭報告論文，於會議的第三天下午，由本實驗室研究生卓琮閔負責歷程約十五分鐘左右的簡報，以投影片介紹相關研究成果，過程中有數名與會學者感到興趣，

並向負責報告的研究生討論研究相關內容，而能透過國際研討會與相關研究領域的學者交談，也讓學生獲益良多。另一篇” Fabrication of Deep Lateral Single-Crystal-Silicon Blaze Micro-grating by Inductively-Coupled-Plasma Reactive Ion Etch”，則是安排為壁報論文，也在壁報展示時間同與會學者交流，獲得寶貴經驗。

而於第三天的晚上所舉辦的餐會，除了可讓與會者放鬆心情外，並可得到更進一步交流的機會，本實驗室也於晚上餐會中，與結識的數位學者交流有關研究上的各種心得；另外主辦單位也在餐會中，向與會者宣傳下一屆研討會的資訊，包括會議的日期、地點以及當地特色，期許眾人能於下屆研討會中，交流更多的研究成果。

二、與會心得

此次研討會中，本實驗室研究生以英文向國際學者報告研究成果，報告情形如圖一所示。另外雖然受限於時間，無法對研究內容作更進一步的詳細介紹，但對相關領域感興趣之學者，也於報告時間之後做進一步的交流討論，如圖二所示。

分享研究成果的過程實在令人感到相當興奮，是一種自我實現的成就感，而透過學術交流世界接軌的過程更是難能可貴。在研討會中各個會議報告都是其精心研究的成果，而利用此次國際交流的機會，吸收這次研討會所提出的嶄新想法，勢必會對學生日後的研究產生很大的影響力。

此外於一些生醫感測器、生醫化學、半導體製程技術等領域上的收穫也頗豐碩，直到最後一天時仍有意猶未盡之感，希望時間能持需停留於此刻。此次參加研討會外參訪的當地人文風情、增進了學術與人文的素養，然而最有趣也最有意義的是進行了許多國民外交，無論是一同前往的教授們、國外學者、對岸朋友或是台灣學生。

圖一、本實驗室研究生於會場內進行報告之照片

圖二、報告結束時與學者討論之照片

在會場也遇到多位台灣教授，一同參與此研討會，如圖三所示，左邊第一位是本人(徐文祥)，右邊第二位是交大電子系鄭裕庭教授，透過討論聽講心得，得到更豐富的經驗分享。

圖三、參加會議之學者合照

三、建議

參加研討會不僅僅是學習，更可以開拓視野深度，探訪當地的風土及其民族精神，這完全取決於心態，唯有將自我放空與縮小，才能吸收更多養分回國深究。在國內告訴研究生該做哪些準備，學生常不能體會原因，透過親身經歷，學生更能體會為何要在出國前，事先將所有口頭報告與海報報告的標題進行了解，挑出有興趣的題目後，到了會場便可快速地進入狀況，迅速地拜訪每個學者，這跟平常在實驗室閱讀文獻有很大的不同，透過當面的問與答可以加速資訊的吸收之外，更可獲取一些文獻中沒有包含到的資訊，對於研究工作相當有幫助；此外也可同時留意國內一同與會的學者，即使研究領域不同，但也可以於會場中結識而替未來的合作留下一個種子。

四、攜回資料名稱及內容

研討會紀念提袋，內含：

(1)議程簡章

(2)會議手冊(內含報告主題與摘要)

(3)光碟(內含論文電子檔)

(4)當地交通資訊

五、發表論文全文或摘要

本實驗室在此次國際研討會議發表的論文共兩篇，謹附於後。

Development of Microbead-based Affinity Biosensor by Insulator-Based Dielectrophoresis

Tsung-Min Chuo[1], Wensyang Hsu[1], Shih-Kang Fan[1,2]
[1]Department of Mechanical Engineering, National Chiao Tung University, TAIWAN
[2]Department of Materials Science and Engineering, National Chiao Tung University, TAIWAN
skfan@mail.nctu.edu.tw

Abstract—**This research describes a high sensitivity microfluidic bead-based immunosensor based on the principle of insulator-based dielectrophoresis (iDEP). An insulator film with small holes between two electrodes creates a nonuniform electric field. By applying appropriate voltage and frequency, the fluorescent beads are concentrated to lower electric field regions due to the difference of dielectric properties. This concentrating step enhances the fluorescence intensity of analytes and decreases the detection limit of immunosenser. In this research, the fluorescence dye is conjugated with streptavidin which has high affinity to biotin. We use biotin-labeled polystyrene beads to bind with streptavidin, therefore, we can further detect fluorescent streptavidin conjugates by a fluorescence microscope. The biotin-labeled polystyrene beads perform not only various chemical characteristics by labeling different functional groups but also offer an increased surface area for antibodies or antigens to immobilize on. Finally, we fabricate a microfluidic bead-based immunosensor with high sensitivity (1 pg/ml), short analysis time (~10 minutes), few sample consumption (~0.5 μl) and without physical microchannel.**

Keywords-component; immunosensor; iDEP; fluorescence

1. Introduction

Immunoassays are biochemical analysis methods based on the high selectivity between antibody and antigen; they normally measure the presence or concentration of a specific substance in solutions or mediums that frequently contain a complex mixture of substances. Moreover, immunoassays are among the most sensitive and specific analytical methods that are routinely used in a clinical laboratory and other biological research applications.

In recent years, a new technique that uses microbeads as a solid support in immunoassays has become usual. There are several advantages in the use of microbeads. First, the microbeads' surface to volume ratio is greater than that of a microtiter plate commonly used in conventional immunoassays. For example, 1 g of microbeads with a diameter of 0.1μm has a total surface area of about 60 m^2 [1]. The large surface area provides a large interface and the reaction field between samples and reagents. The sensitivity of immunoassays would be increased as a result of the higher efficiency of the immunoreactions between the immobilized antibody and the antigen present in a continuous flow. In addition, the reaction rate may be increased because of the greater reaction field.

Second, the immunoassays which use microbeads as a solid support can be easily integrated into a microfluidic chip. The samples and reagents that used in immunoassays can be easily transported in a fluidic system by a syringe pump or another way. Third, there are various available surface modifications for microbeads. DNA, RNA, antibodies, antigens and a vast number of other biological molecules can be easily fixed on the surface of microbeads. Moreover, transportation and analysis in a fluidic system is easy [2].

Furthermore, the dynamic condition that utilizing both diffusion and convectional forces to deliver or mix samples with reagents in microfluidic system. In contrast, conventional immunoassay on a microtiter plate, likes enzyme-linked immunosorbent assay (ELISA), is a static condition that merely depends on diffusion of the molecules for interaction and binding.

Microfluidic technology is widely used in immunoassays available to improve the analytical characteristic performances, such as short analysis time, high reliability and high detecting sensitivity, easy handling and low consumption of reagents [3]. However, a retention method is necessary for trapping or fixing microbeads in microfluidic system in order to avoid the microbeads washing away in the microfluidic system. For example, microbeads can be trapped by arrayed microstructures [4]-[6], Kitamori and coworkers fabricated a dam structure for retaining polystyrene microparticles in a glass-based microchannel [6]. Magnetic beads are also used for immunoprotein support and separation, since these beads can be easily manipulated in the channel by applying a magnetic field [7]-[9]. Dielectrophoresis [10][11], and electrostatic forces [12][13] are another way to be a retention method.

Sensitivity means the lowest concentration or the smallest amount of analytes that can be detected above the baseline, which is perhaps the most widely touted measures of an assay since it is easy quantified. Compared to conventional immunoassays, those relying on fluorescence detection, are known to be highly sensitive [14]. They have the potential that can replace the traditional ELISA technique if the fluorescence signal arising from fluorophores bound with analytes can be effectively reinforced.

In this research, we can enhance the fluorescence intensity in a simple way instead of complex chemical operations. The fluorescence intensity can be increased by concentrating beads. We have developed a fluorescent bead-based immunoassay using iDEP adapted from existing ELISA. This microfluidic

bead-based immunosensor has high sensitivity, short analysis time, few sample consumption and without any microchannel.

2. Theory

2.1. Dielectrophoresis

Dielectrophoresis (DEP) is an electrokinetic phenomenon which can drive particles by using electrodes instead of moving actuators. A dielectric particle suspending in a solution would be affected by a force caused by the interaction between the spatially inhomogeneous electrical fields causing polarization. The DEP force has been widely used to manipulate, transport, separate and sort different types of particles.

DEP can be classified into two types: positive DEP (p-DEP) and negative DEP (n-DEP). Particles are attracted to the region of a stronger electric field with the p-DEP force because their permittivity is greater than that of the solution. In contrast, particles are attracted to the region of a weaker electric field with the n-DEP force because their permittivity is smaller than that of the solution. In addition, p-DEP [15][16] and n-DEP [17][18] have been used to manipulate particles and biological cells with microelectrode systems.

The DEP force, F_{DEP}, on a suspended spherical particle in a solution is given by

$$F_{DEP} = 2\pi\varepsilon_m a^3 \,\mathrm{Re}(f_{CM})\nabla E^2{}_{RMS}, \qquad (1)$$

where a is the particle radius [m], ε_m is the permittivity of the suspension solution [F/m], E_{RMS} is the root-mean-square electric field [V/m], ∇ is the del vector operator, and $\mathrm{Re}(f_{CM})$ is the real part of the Clausius-Mossotti factor, given by

$$f_{CM} = \frac{\tilde{\varepsilon}_p - \tilde{\varepsilon}_m}{\tilde{\varepsilon}_p + 2\tilde{\varepsilon}_m}, \qquad (2)$$

where $\tilde{\varepsilon}_p$ is the complex permittivity of the particle, and $\tilde{\varepsilon}$ is given by

$$\tilde{\varepsilon}_m = \varepsilon_m - \frac{\sigma_m}{\omega} j, \qquad \tilde{\varepsilon}_p = \varepsilon_p - \frac{\sigma_p}{\omega} j, \qquad (3)$$

where σ is the conductivity [S/m], ε is the permittivity, ω is the angular frequency and j equals $\sqrt{-1}$.

2.2. Insulator-based dielectrophoresis

Insulator-based (electrodeless) dielectrophoresis (iDEP) is a technology to produce the nonuniform electrical field by insulators for driving DEP. Hence iDEP would avoid the problems caused by electrodes.

In this research, iDEP is used to collect fluorescent beads on a specific device which includes two electrodes with a patterned insulator film in between as shown in Fig. 1. When voltage is applied on the device, the charged fluorescent beads are gathered at the region of weaker electric field on the insulator film, so that the beads collection can be completed by the n-DEP force. The fluorescence signal will be enhanced by concentrating fluorescent beads. The method can increase fluorescence intensity and sensitivity. Our device is based on the iDEP technique to detect a limited amount of streptavidin.

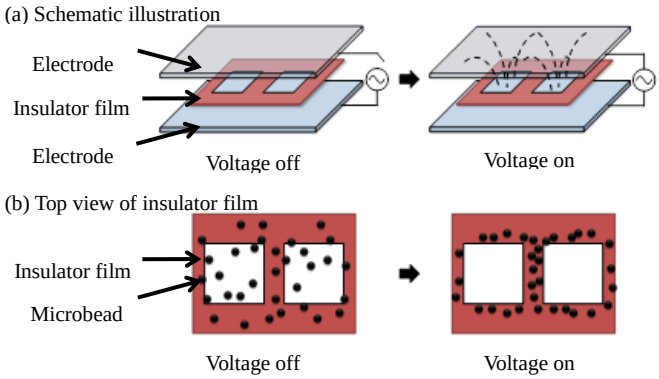

Fig. 1. Principle behind the assay methodology, combining the insulator film and the n-DEP-based manipulation techniques. (a) Using insulator film to

3. Experiment

3.1. Fabrication

Indium tin oxide (ITO) is one of the most widely used transparent conducting oxides because of its electrical conductivity and optical transparency, as well as the ease of depositing and pattering. The device was fabricated on glass substrate with deposited ITO thin film. The dielectric layer of 2 μm Parylene C was deposited on ITO thin film by chmical vaporization deposition (CVD). The hydrophobic layer of Teflon is spin-coated onto the dielectric layer for increasing the contact angle of droplets.

The insulator film was fabricated by dry film photoresist (PerMX3020, DuPont). The pattern on the PerMX dry film is shown in Fig. 2. The pattern consists 25 squares arranged in a 5 ×5 array. The length of the squares is 35 μm and the interval between the squares is 60 μm. To fabricate it, a PerMX dry film was baked and is exposed by UV light (350-400 nm). Afterward, the PerMX dry film was developed by PerMX developer and rinsed by IPA.

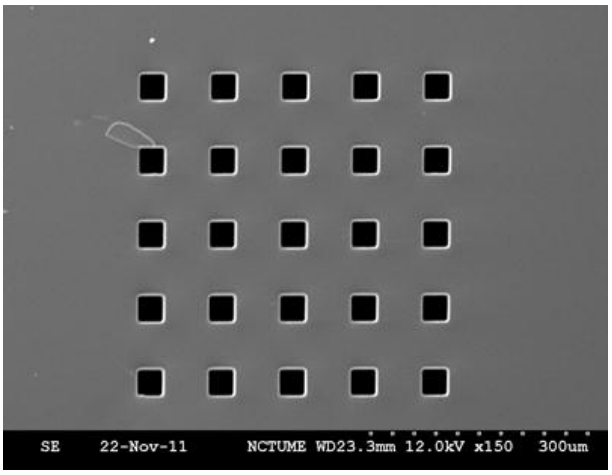

Fig. 2. SEM photo of the patterned PerMX dry film.

3.2. Reagents and Materials

Biotin covalently coupled to Fluoresbrite® YG fluorescent microbeads (2μm diameter) was purchased from Polysciences, Inc. (U.S.A.). The biotin-labeled polystyrene beads were dispensed into a microcentrifuge tube and centrifuged at 10000 ×G for 5 minutes. The supernatant in the tube was then rded. The beads are resuspended in PBS/BSA binding buffer. These steps will be repeated three times to wash the microsbeads. After the last washing, the beads can be resuspended to any volume, however higher concentrations usually work better (at least 5×10^8 particles/ml).

Rhodamine B labeled streptavidin purchased from Invitrogen (U.S.A.) was incubated with the processed beads for 30 minutes at 4˚C to ensure that the reaction between two species was sufficient. The tube was centrifuged for 5 minutes and the supernatant in the tube was discarded. The beads are resuspended in PBS/BSA binding buffer. After repeating three times, the beads were ready for use in the following experiment.

3.3. Experiment Setting

Double side tapes were pasted between the ITO glass plate and the insulator film as spacers. A 0.5 μl droplet was created by a pipette. Cross section of the experiment setting is shown in Fig. 3. AC voltage was applied to the sandwich constructer from a function generator. Finally, wires are connected between the chip and the control circuits. The condition of concentrated beads can be observed under a fluorescence microscope.

AC signal is produced by a function generator and passed through an amplifier to the electrodes. The electrodes were connected to a PC via an I/O card (DAQCard-USB6251). The signal is controlled with LabVIEW software (National Instruments). Detection processes was visualized by a fluorescence microscopy (IX71, Olympus) equipped with a CCD camera. The fluorescence images were analyzed by image analysis software (Image Pro Plus).

4. Results and Discussion

4.1. Concentrate Beads

By applying voltage, the beads would be concentrated of the gap between two square holes of the insulator film by the n-DEP force. In this experiment, two different fluorescence dyes are labeled on biotin-labeled polystyrene beads and

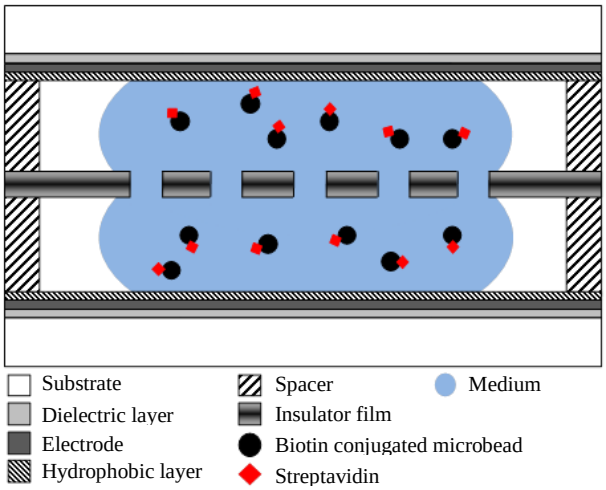

Fig. 3. The cross section of experiment construction.

streptavidin separately. Therefore, we would observe the condition of biotin-labeled polystyrene beads and streptavidin simultaneous by using different optical filter, respectively. The results are shown in Fig. 4 and the operation time was 15 minutes.

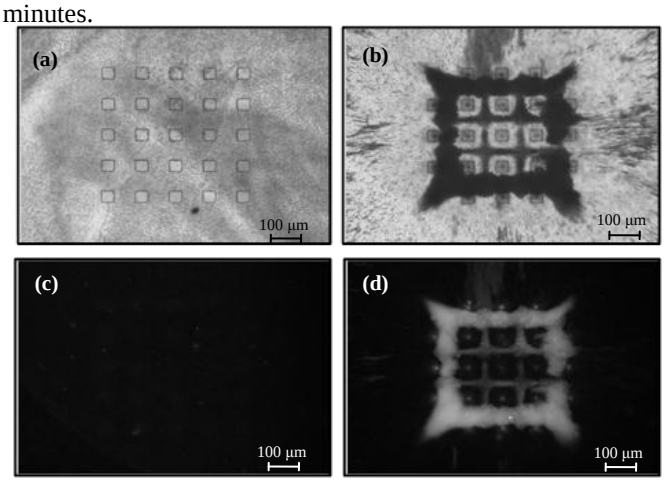

Fig. 4. The photos of concentrated beads on insulator film. (a) Before apply voltage (bright field). (b) Apply voltage to concentrate beads after 15 minutes (bright field). (c) Before apply voltage (fluorescence field). (d) Apply voltage

4.2. Operation Time

The fluorescence intensity of concentrated beads approaches to a limit after a long time. It is important to determine how

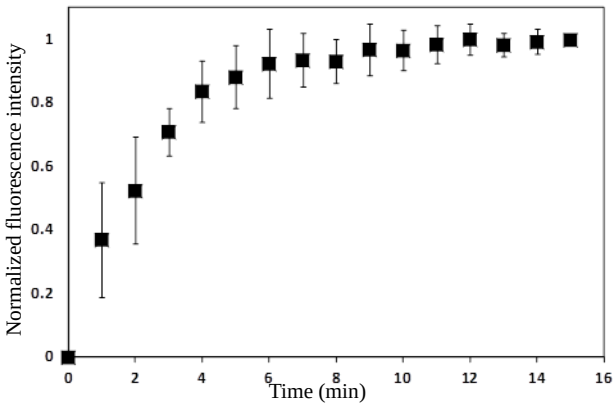

Fig. 5. The measured intensity of concentrated fluorescent beads plotted along

long we need to concentrate beads. For quantitative evaluation of concentrated beads, the value of fluorescence intensity was calibrated to be 0 for the initial state and 1 for the final state. We applied a 140 V_{RMS} voltage at 100 kHz and analyzed the captured photos caught during operation. The results are shown

in Fig. 5. From the results, the fluorescence intensity becomes stable about 10 minutes. The correlation coefficient for these 15 samples is ~0.92, which seems to be rather high for an immunoassay.

4.3. **Results**

The fluorescence intensity increased while the concentration of fluorescent dye increased. In this research, we used fluorescent beads and Rhodamine B labeled streptavidin. For quantitative evaluation of the relation between intensity and the concentration of Rhodamine B labeled streptavidin. First, we choose a value of fluorescent beads' fluorescence intensity. Then, the value of streptavidin's fluorescence intensity divides by this number. Finally, we can get a concentration-fluorescence intensity graph and is summarized in Fig. 6. Concentrations of the Rhodamine B labeled streptavidin ranges from 1 pg/ml to 1 ng/μl and the determination limit is 1 pg/ml.

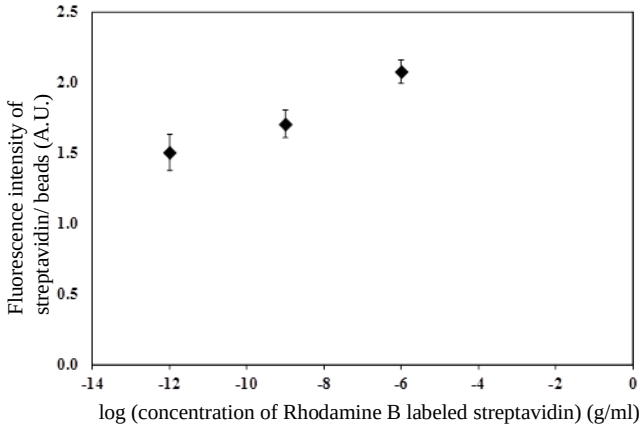

Fig. 6. The calibration curve of Rhodamine B labeled streptavidin.

5. Conclusion

In this paper, we increase the sensitivity of a bead-based immunosensor by concentrating beads instead of complex chemical operations. The concentration step by iDEP is finished less than 10 minutes and increases the fluorescence under 140 V_{RMS} at 100 kHz. We anticipate that this mechanism may be useful in Pico-scale for clinical diagnosis or other biological research applications.

ACKNOWLEDGMENT

This work is supported by the National Science Council of Taiwan under grant NSC-100-2120-M-009-009.

REFERENCES

[1] E. Verpoorte, "Beads and chips: new recipes for analysis," *Lab Chip*, vol. 3, pp.60N-68N, 2003.

[2] C.J. Lim, and Y. Zhang, "Bead-based microfluidic immunoassays: The next generation," *Biosens. Bioelectron.*, vol. 22, pp. 1197-1204, 2007.

[3] A. Bange, H.B. Halsall, and W.R. Heiniman, "Microfluidic immunosensor systems," *Biosens. Bioelectron.*, vol. 20, pp. 2488-2503, 2005

[4] H. Andersson, W.v.d. Wijngaart, P. Enoksson, and G. Stemme, "Micromachined flow-through filter-chamber for chemical reactions on beads," *Sens. Actuators, B*, vol. 67, pp. 203-208,2000.

[5] K. Sato, M. Tokeshi, T. Odake, H. Kimura, T. Ooi, M. Nakao, and T. Kitamori, "Integration of an immunosorbentassay system: analysis of secretory human immunoglobulin A on polystyrene beads in a microchip," *Anal. Chem.*, vol. 72, pp. 1144-1147, 2000.

[6] K. Sato, M. Yamanaka, H. Takahashi, M. Tokeshi, H. Kimura, and T. Kitamori, "Microchip-based immunoassay system with branching multichannels for simultaneous determination of interferon- γ ," *Electrophoresis*, vol. 23, pp. 734-739, 2002.

[7] J.W. Choi, K.W. Oh, J.H. Thomas, W.R. Heineman,H.B. Halsall, J.H. Nevin, A.J. Helmicki, H.T. Henderson, and C.H. Ahn, "An integrated microfluidic biochemical detection system with magnetic bead-based sampling and analysis capabilities," *Lab Chip*, vol. 2, pp. 27-30, 2002.

[8] C.A. Wijayawardhana, S. Purushothama, M.A. Cousino, H.B. Halsall, and W.R. Heineman, "Rotating disk electrode amperometric detection for a bead-based immunoassay," *J. Electroanal. Chem.*, vol. 468, pp. 2-8, 1999.

[9] E. Zacco, M.I. Pividori, S. Alegret, R. Galve, and M.P. Marco, "Electrochemical magnetoimmunosensing strategy for the detection of pesticides residues," *Anal. Chem.*, vol. 78, pp. 1780-1786, 2006.

[10] T. Yasukawa, M. Suzuki, T. Sekiya, Shiku H, and Matsue T, "Flow sandwich-type immunoassay in microfluidic devices based on negative dielectrophoresis," *Biosens. Bioelectron.*, vol. 22, pp. 2730-2736, 2007.

[11] D. Holmes, J.K. She, P.L. Roach, and H. Morgan, "Bead-based immunoassays using a micro-chip flow cytometer," *Lab Chip*, vol. 7, pp. 1048-1056, 2007.

[12] V. Sivagnanam, B. Song, C. Vandevyver, and M.A.M. Gijs, "On-Chip Immunoassay Using Electrostatic Assembly of Streptavidin-Coated Bead Micropatterns," *Anal. Chem.*, vol. 81, pp.6509-6515, 2009.

[13] V. Sivagnanam, A. Bouhmad, F. Lacharme, C. Vandevyver, and M.A.M. Gijs, "Sandwich immunoassay on a microfluidic chip using patterns of electrostatically self-assembled streptavidin-coated beads," *Microelectron. Eng.*, vol. 86, pp.1404-1406, 2009.

[14] R.S. Yalow, and S.A. Berson, "Immunoassay of endogenous plasma insulin in man", *J.Clin. Invest.*, vol. 39, 1157-1175, 1960.

[15] D.S. Gray, J.L. Tan, J. Voldman, and C.S. Chen, "Dielectrophoretic registration of living cells to a microelectrode array," *Biosens. Bioelectron.*, vol. 19, pp. 1765-1774, 2004.

[16] S. Masuda, M. Washizu, and T. Nanbu, "Novel method of cell fusion in field constriction area in fluid integration circuit," *IEEE Trans. Ind. Appl.*, vol. 25, pp. 732-737, 1989.

[17] M. Suzuki, T. Yasukawa, T. Mase, D. Oyamatsu, H. Shiku, and T. Matsue, "Dielectrophoretic Micropatterning with Microparticle Monolayers Covalently Linked to Glass Surfaces," *Langmuir*, vol. 20, pp. 11005-11011, 2004.

[18] T. Matsue, N. Matsumoto, and I. Uchida, "Rapid micropatterning of living cells by repulsive dielectrophoretic force," *Electrochim. Acta*, vol. 42, pp. 3251-3256, 1997

Fabrication of Deep Lateral Single-Crystal-Silicon Blaze Micro-grating by Inductively-Coupled-Plasma Reactive Ion Etch

Y. H. Lin[1,2], C. J. Weng [2], C. Y. Su[2], W. Hsu[1]

[1] Department of Mechanical Engineering, National Chiao Tung University , Hsinchu, Taiwan, R.O.C.

[2] Instrument Technology Research Center, National Applied Research Laboratories, Hsinchu, Taiwan, ROC.

yhlin@itrc.narl.org.tw

***Abstract*—This paper presents a method by using a compensative structure assisted to fabricate deep lateral single-crystal-silicon (SCS) blaze micro-grating at Inductively-Coupled-Plasma Reactive Ion Etch (ICP-RIE). Due to the high resolution of blaze micro-grating, it's hard to maintain the teeth structure of blaze micro-grating under deep silicon etch in ICP-RIE process. Here, the independent rectangular structure and symmetrical structure to micro-grating is designed to obstruct the non-vertical plasma ion to etch the sidewall of micro-grating structure and to get better the profile control at deep micro-grating structure. The lateral silicon blaze micro-grating with 100 μm thickness by compensative structure assisted etch process have been successfully demonstrated this method.**

Keywords-blaze graing; Inductively-Coupled-Plasma Reactive Ion Etch (ICP-RIE).

1. Introduction

Due to excellent material properties of the single-crystal-silicon (SCS), the lateral silicon blaze micro-grating have potential to integrate the MEMS sensors and actuators [1]. The micro-grating is an important optical device, especially in applications of optical coherence tomography (OCT), micro-spectrometer, tunable laser, dense wavelength division multiplexer (DWDM) etc. Profile control of teeth structures is important issue in manufacturing lateral blaze micro-grating. In anisotropic silicon etching, under the Bosch patent, sequentially alternating etch and passivation cycles can easily achieve high-aspect-ratio silicon structures [2,3]. Many fabrication parameters such as uniformity, etch lag and geometrical effect in ICP-RIE have been investigated to obtain high-aspect-ratio structures [4-8]. There is rare research to discuss the corner structure like teeth of micro-grating under deep ICP-RIE etching. In fabricating lateral SCS blaze micro-grating by ICP-RIE process, the teeth structure of micro-grating can't still maintain under deep etching. In this paper, we propose a method using a compensative structure assisted etch process to fabricate better profile of grating at the deep ICP-RIE.

2. Design

The experimental study is performed in the STS Multiplex ICP-RIE here. This study generates the source plasma of an inductively coupled coil by a 1kW 13.56 MHz R.F generator, and uses another 13.56MHz generator as a platen power to independently control the bias potential of the wafer relative to the source plasma. The fabrication process maintains at low temperature using helium as cooling gas supplied to the backside of the wafer. Sulfur hexafluoride (SF_6) and octafluorocyclobutane (C_4F_8) are used as the main etch and passivation gases, respectively.

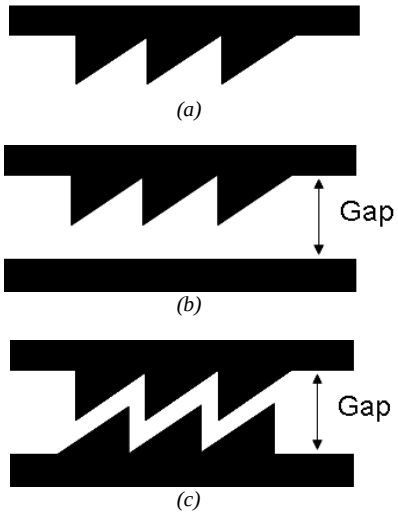

Fig. 1. Micro-grating (a)without compensative structure, (b)with rectangular compensative structure and (c) with symmetrical compensative structure to assisted profile control in ICP-RIE etching.

2.1. Concept Design

In the proposed method, a compensative structure near silicon blaze micro-grating structure is designed to assist etching process in ICP-RIE. Here, the lateral blaze micro-grating structure with 8.9 degrees blaze angle, 10 μm periodic grating structures as the critical device is used to investigate the profile control of teeth structures after ICP-RIE deep etch, as shown in figure 1(a). The rectangular compensative structure and symmetrical compensative structure near micro-grating structure that assisted ICP-RIE etching is design, as shown in figure 1(b) and figure 1(c). The gap between teeth structures and compensative structure is 5 μm.

2.2. **Fabrication Process**

Figure 2 schematically shows the fabrication flowchart using the compensative structure assisted ICP-RIE etch in fabricating lateral silicon blaze micro-grating. First, the negative photo-resist (SU-8 2002) is spun and patterned as an etch mask on a SOI wafer, as shown in figure 2(a). The SU-8 is baked by 95℃ 20minutes to enhance the resist the plasma ion etching. The lateral silicon blaze micro-grating structure is etched by Bosch silicon cyclic anisotropic etch, as shown in figure 2(b). Finally, the compensative structure is removed by hydrofluoric acid (HF) wet etch.

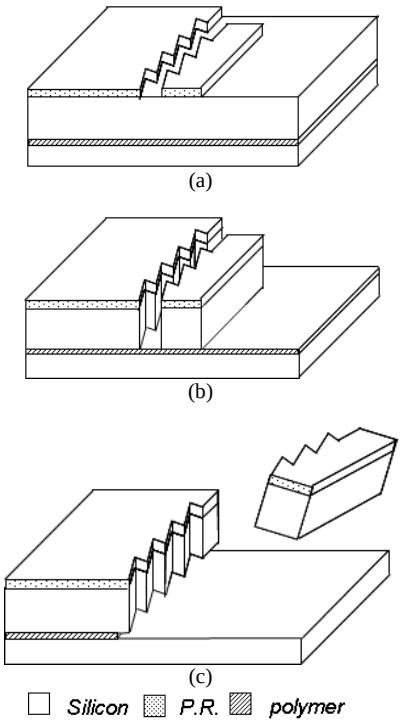

Fig. 2. Fabrication flowchart of lateral silicon blaze micro-grating using compensative structure assisted RIE etch.

3. Experimental results and disscussions

3.1. **Process results**

This paper uses lateral silicon blaze micro-grating without/with rectangular and symmetrical compensative structure to discuss the profile control at the teeth of micro-grating structure at deep ICP-RIE. The compensative structure is a temporary structure at fabrication process. So, the compensative structure is designed as independent structure that easily to remove after anisotropic etching. The SOI wafer with 100 μm device thickness is used here. The silicon cyclic anisotropic etching recipe used in this study, which is based on Bosch anisotropic etching method, is 800/12 W source/bias power, 130/13 sccm SF_6/O_2 flow rate, 12 seconds in etching step, and 800/0 W source/bias power, 85 sccm C_4F_8 flow rate, 8 seconds in passivation step. Etch rate is about 2.3 μm /minutes.

Since the Bosch patent, etch and passivation cyclic mechanism developed, the high-aspect-ratio anisotropic silicon structures can be easily achieved. The pattern from photo-resist to silicon is fine transferred at the beginning etch, even in corner structures. But the structures at the corner can't be maintained as original designed under deep etch. This is seriously issue influenced efficiency at some devices like optical grating that need accurate structure's profile.

Figure 3(a) shows the scanning electron microscope (SEM) photograph of the lateral silicon blaze micro-grating under ICP-RIE etching. The teeth structures of micro-grating are measured by Atomic Force Microscopy (AFM) and profile photograph, as shown in figure 3(b) and figure 3(c). The profile of the teeth is approach flat under 50 μm depth**.** The efficiency of dispersion of light at grating structures is low caused by not bad teeth structures.

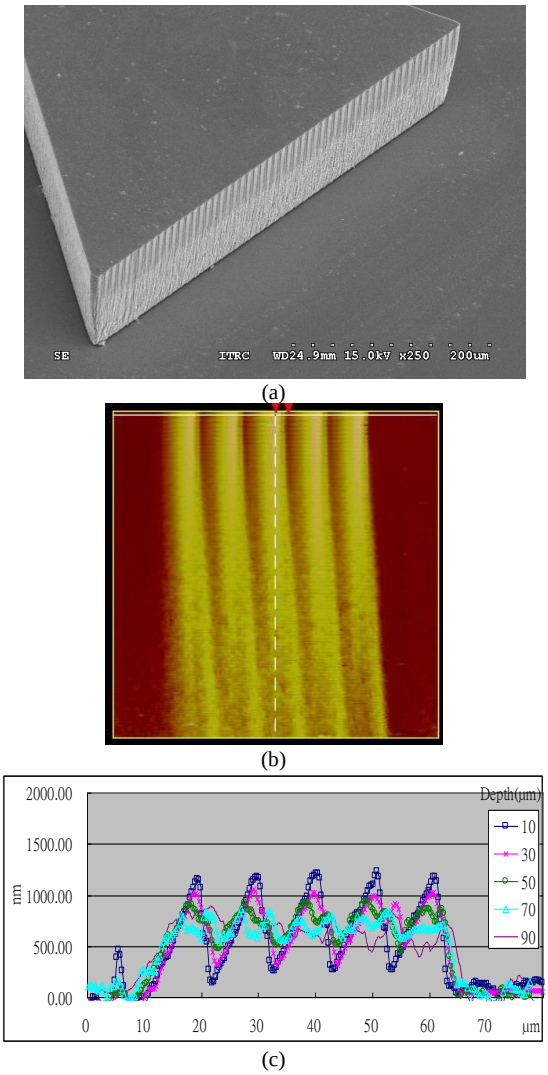

Fig. 3. The lateral silicon blaze micro-grating (a)SEM, (b)AFM, (c)profile photography under ICP-RIE etching without any compensative structure.

In ICP-RIE etching, the structures at the corner is hard be maintained after deep etch. Most plasma ion has been moved vertically by bias voltage attraction and performed spontaneous etch to the base silicon. But, some plasma applied non-vertical movement, due to the

collision between plasma. The non-vertical movement plasma has spontaneous etching reactions with silicon material at the sidewall. The etching of silicon at the sidewall becomes serious at deep position which can explain the damage of the grating structure at deep position in figure 3(a). Enlarged bias voltage and lowered process chamber pressure can slightly reduce the non-vertical plasma ion. But, it is not effective method to solve this problem.

In this paper, an independent and compensative structure near the blaze micro-grating is design to assist the corner profile control. This compensative structure not only can obstruct the most non-vertical plasma to etch the silicon at the sidewall of the grating, but also can reduce the effect of etch

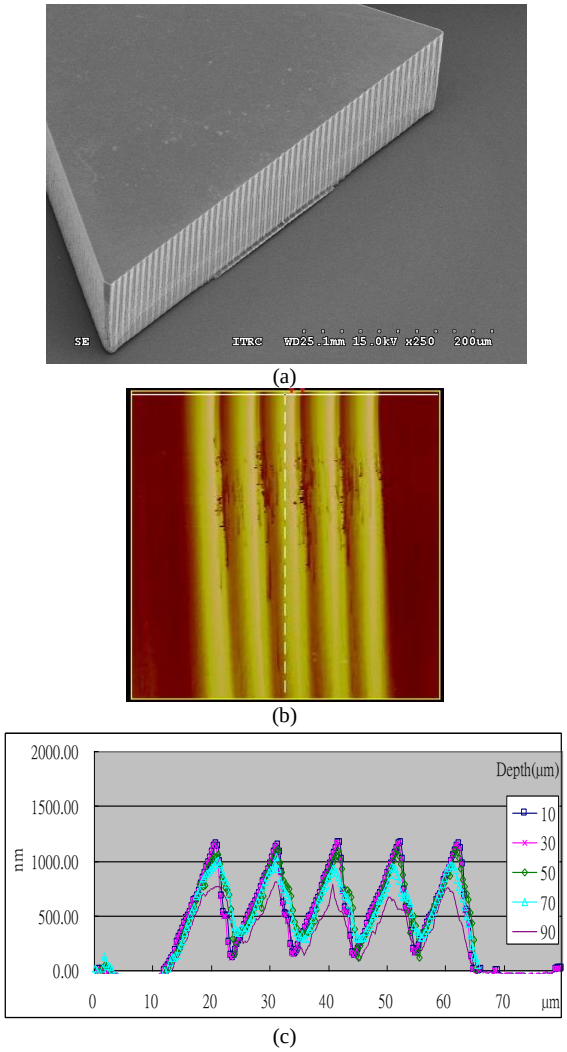

Fig. 4. The lateral silicon blaze micro-grating (a)SEM, (b)AFM, (c)profile photography under ICP-RIE etching with rectangular compensative structure assisted etch.

lag around the teeth structures.

A rectangular compensative structure near blaze micro-grating structure is design, as shown in figure 1(b). After anisotropic silicon etch and rectangular compensative structure removal, the teeth structures at the deep position obviously have been improved, as shown in figure 4(a). The AFM and profile photograph of teeth are shown in figure 4(b). and figure 4(c). The profile of teeth structures at 70 μm deep position is similar to at 10 μm deep. The teeth structures still have maintained even in 90 μm deep.

The SEM photography of grating with symmetrical compensative structure assisted etch is shown in figure 5(a). The AFM and profile photograph of teeth are shown in figure 5(b). and figure 5(c). The profile of the teeth structures with symmetrical compensative structure is also obviously better than without compensative structure.

Although, the compensative structure can improve the profile of teeth of the grating structures at deep etch, but some extra defects have be found at sidewall silicon at 30~50 μm

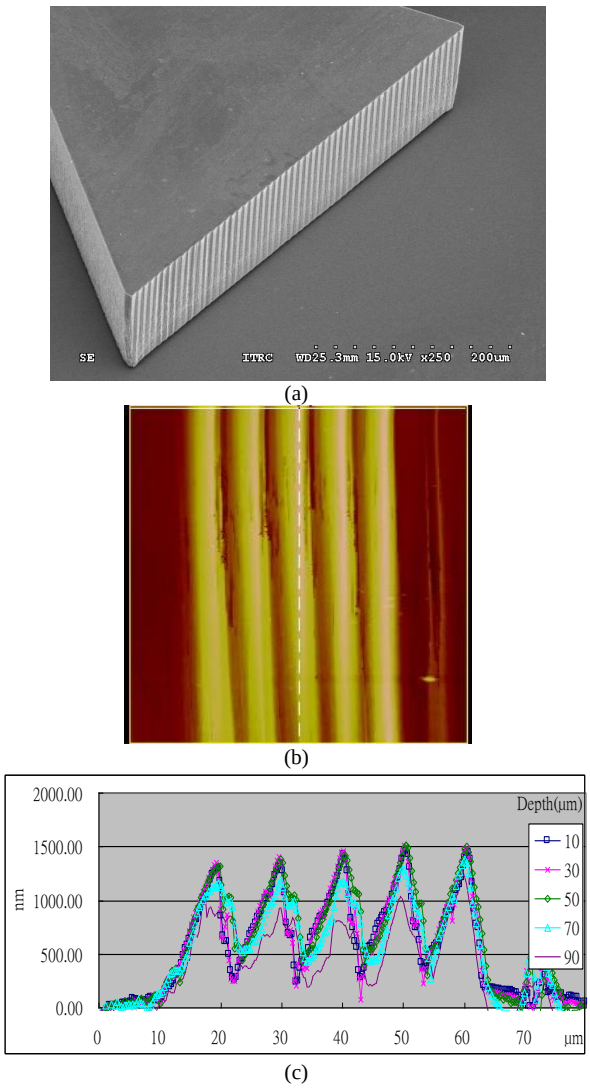

Fig. 5 The lateral silicon blaze micro-grating (a)SEM, (b)AFM, (c)profile photography under ICP-RIE etching with symmetrical

deep as shown in AFM photography, as shown in figure 4(b) and figure 5(b). These defects didn't happen at grating without compensative structure, as shown in figure 3(b). These defects of the sidewall caused by reflected ion from the mask side on the compensative structure [4].

3.2. Optical measurement results

The schematic diagram of measurement setup is shown in figure 6. The measurement equipments include 6W

power 450~2000nm wavelength supercontinnum light source, cylindrical lens for focusing output spectrum, CMOS linear sensor arrays for optical amplitude measurement.

Figure 7 shows the optical measurement results of lateral blaze micro-grating without compensative structure assisted etch and with rectangular/symmetrical compensative structure

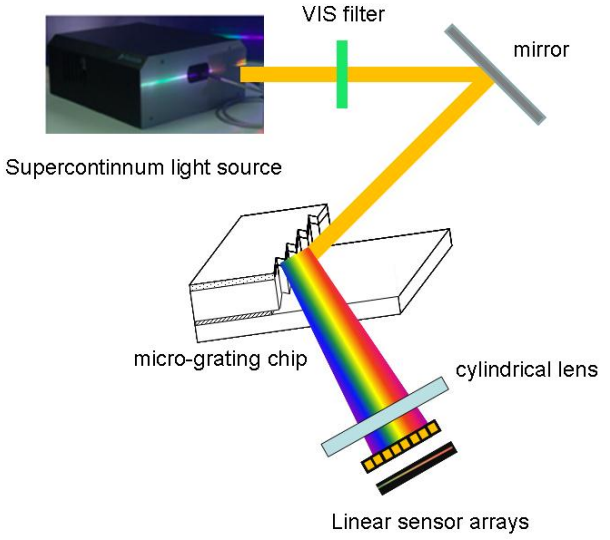

Fig. 6 The schematic diagram of optical measurement.

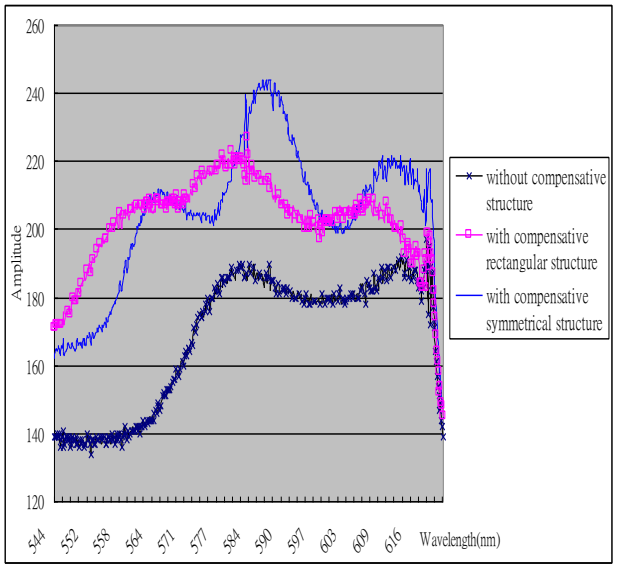

Fig. 7 Optical amplitude of grating without, with rectangular assisted etch. The amplitude of background is 120 measured by the same CMOS linear sensor arrays. The amplitude of micro-grating with compensative structure assisted profile control is obviously higher than without compensative structure. The amplitude of grating with symmetrical compensative structure is higher than with rectangular compensative structure. The grating with symmetrical compensative structure let the opening gap be the same around the teeth of the grating. So, the symmetrical compensative structure with grating not only can block non- vertical plasma to etch the silicon material at the depth position, but avoiding etch lag effect around the teeth structures.

4. Summary

A method to fabricate the deep lateral SCS blaze micro-grating by add a compensative structure near the micro-grating to assist ICP-RIE etch has been proposed. The rectangular and symmetrical compensative structure is design to obstruct the non-vertical plasma ion etch and reduce the etch lag effect. The better profile of the grating structure with 100 μm has been successfully fabricated using the symmetrical compensative structure method.

ACKNOWLEDGMENT

This work is supported by Instrument Technology Research Center of National Applied Research Laboratories for providing fabrication facilities and technical supports.

REFERENCES

K. E. Peterson, "Silicon as a mechanical material", *Proc. IEEE*, vol.70, pp. 420-457, 1982.

[1] F. Larmer, and A. Schilp, " Method of anisotropically etching silicon ", German Patent DE4241045C1, USA patents 4855017 and 478472.

[2] A.M. Hynes, H. Ashraf, J.K. Bhardwaj, J. Hopkins, I. Johnston, J.N. Shepherd, "Recent advances in silicon etching for MEMS using the ASE process", *Sensors and Actuators*, vol. 74, pp. 13–17, 1999.

[3] G. Marcos, A. Rhallabi, and P. Ranson, "Monte Carlo simulation method for etching of deep trenches in Si by a SF6/2 plasma mixture", *J. Vac. Sci. Technol.* A 21(1), 2003.

[4] C. K. Chung, "Geometrical pattern effect on silicon deep etching by an inductively coupled plasma system", *J. Micromech. Microeng.* vol. 14, pp. 656–662, 2004.

[5] C. K. Chung, H. C. Lu, and T. H. Jaw, "High aspect ratio silicon trench fabrication by inductively coupled plasma", *Microsystem Technologies*, vol. 6, pp. 105-108, 2000.

[6] J. Yeom, Y. Wu, J. C. Selby, and M. A. Shannon, "Maximum achievable aspect ratio in deep reactive ion etching of silicon due to aspect ratio dependent transport and the microloading effect", *J. Vac. Sci. Technol. B.* 23(6), pp. 2319-2329, 2005.

[7] B. Wu, A. Kumar, and S. Pamarthy, "High aspect ratio silicon etch: A review", *JOURNAL OF APPLIED PHYSICS*, 108, 051101 _2010.

國科會補助計畫衍生研發成果推廣資料表

日期:2012/10/01

國科會補助計畫	計畫名稱: 以高分子作為感應偶合電漿反應離子蝕刻側壁保護層以製作單晶矽懸浮微結構之快速製程平台研發
	計畫主持人: 徐文祥
	計畫編號: 100-2221-E-009-034- 學門領域: 加工與製造

無研發成果推廣資料

100 年度專題研究計畫研究成果彙整表

計畫主持人：徐文祥	**計畫編號：**100-2221-E-009-034-
計畫名稱：以高分子作為感應偶合電漿反應離子蝕刻側壁保護層以製作單晶矽懸浮微結構之快速製程平台研發	

成果項目			量化			單位	備註（質化說明：如數個計畫共同成果、成果列為該期刊之封面故事...等）
			實際已達成數（被接受或已發表）	預期總達成數(含實際已達成數)	本計畫實際貢獻百分比		
國內	論文著作	期刊論文	0	0	100%	篇	
		研究報告/技術報告	0	0	100%		
		研討會論文	0	0	100%		
		專書	0	0	100%		
	專利	申請中件數	0	0	100%	件	
		已獲得件數	0	0	100%		
	技術移轉	件數	0	0	100%	件	
		權利金	0	0	100%	千元	
	參與計畫人力（本國籍）	碩士生	1	0	30%	人次	
		博士生	3	3	100%		
		博士後研究員	0	0	100%		
		專任助理	0	0	100%		
國外	論文著作	期刊論文	1	2	100%	篇	Lin, Yu-Hsin and Hsu, Wensyang*, 2012, ’Polymer as the protecting passivation layer in fabricating suspended SCS structures at both anisotropic and isotropic etching’, J. Micromech. Microeng. 22, 045015. (SCI, IF:2.276, N/M=12/132)
		研究報告/技術報告	0	0	100%		
		研討會論文	2	2	100%		
		專書	0	0	100%	章/本	
	專利	申請中件數	0	0	100%	件	
		已獲得件數	0	0	100%		

	技術移轉	件數	0	0	100%	件	
		權利金	0	0	100%	千元	
	參與計畫人力（外國籍）	碩士生	0	0	100%	人次	
		博士生	0	0	100%		
		博士後研究員	0	0	100%		
		專任助理	0	0	100%		
其他成果 (無法以量化表達之成果如辦理學術活動、獲得獎項、重要國際合作、研究成果國際影響力及其他協助產業技術發展之具體效益事項等，請以文字敘述填列。)		無					

	成果項目	量化	名稱或內容性質簡述
科教處計畫加填項目	測驗工具(含質性與量性)	0	
	課程/模組	0	
	電腦及網路系統或工具	0	
	教材	0	
	舉辦之活動/競賽	0	
	研討會/工作坊	0	
	電子報、網站	0	
	計畫成果推廣之參與（閱聽）人數	0	

國科會補助專題研究計畫成果報告自評表

請就研究內容與原計畫相符程度、達成預期目標情況、研究成果之學術或應用價值（簡要敘述成果所代表之意義、價值、影響或進一步發展之可能性）、是否適合在學術期刊發表或申請專利、主要發現或其他有關價值等，作一綜合評估。

1. 請就研究內容與原計畫相符程度、達成預期目標情況作一綜合評估

■達成目標

□未達成目標（請說明，以 100 字為限）

□實驗失敗

□因故實驗中斷

□其他原因

說明：

2. 研究成果在學術期刊發表或申請專利等情形：

論文：■已發表 □未發表之文稿 □撰寫中 □無

專利：□已獲得 □申請中 ■無

技轉：□已技轉 □洽談中 ■無

其他：(以 100 字為限)

3. 請依學術成就、技術創新、社會影響等方面，評估研究成果之學術或應用價值（簡要敘述成果所代表之意義、價值、影響或進一步發展之可能性）(以 500 字為限)

本計畫發展出感應耦合電漿離子蝕刻（ICP-RIE）之體型微加工快速製程平台，其特色是以高分子作為非等向性與等向性乾蝕刻保護層，來製作單晶矽懸浮結構製程平台技術（Polymer Passivation Layer for Suspended structures Etching , PoPLSE)，除黃光製程外，其餘製程均整合在 ICP-RIE 機台中完成。其優點包含低溫製程、製程簡化、使用機台少及製程快速。本計畫成功建立優化後之基本參數，於非等向性蝕刻可得到深寬比達 30 且垂直度 89 ±1°深寬比結構；於等向性蝕刻的部分，則探討高分子之保護效果，在不同結構開口尺寸下，高分子薄膜沈積、底部高分子薄膜去除及等向性蝕刻之各項參數關係，並成功製作出梳狀懸浮結構，成功驗證此快速製程平台之可行性。